

Review

Removal of NO_x by photocatalytic processes

Janusz Lasek^{a,b}, Yi-Hui Yu^a, Jeffrey C.S. Wu^{a,*}

^a Department of Chemical Engineering, National Taiwan University, Taipei 10617, Taiwan

^b Institute for Chemical Processing of Coal, ul. Zamkowa 1, 41-803 Zabrze, Poland

ARTICLE INFO

Article history:

Received 17 April 2012

Received in revised form 15 August 2012

Accepted 21 August 2012

Available online 27 August 2012

Keywords:

Nitric oxide

Photocatalysis

Selective catalytic reduction

deNO_x

ABSTRACT

The photocatalytic methods for nitrogen oxides removal were recently very intense areas of scientific research. Photo-deNO_x processes offer interesting ways for abatement of these harmful gases. This review describes several methods for removing NO by photocatalytic reactions. These methods can be classified into three major groups: photo selective catalytic reduction (photo-SCR), photo-oxidation and photo-decomposition. The application of photocatalysts and photo-processes for NO_x abatement in real-scale cases are presented. The fast-growing development of these methods is revealed by the large number of issued patents in photo-deNO_x applications. The mechanism of NO creation and the traditional methods (primary and secondary) of NO_x removal are summarized and discussed. A cooperative system that combines the traditional (thermal) process and a photo-process is then proposed for improving NO_x removal efficiency.

© 2012 Elsevier B.V. All rights reserved.

Contents

1. Introduction.....	30
1.1. Mechanism of NO generation.....	30
2. Methods for NO _x removal.....	31
2.1. Primary methods.....	31
2.2. Secondary methods.....	31
2.2.1. Reduction.....	31
2.2.2. Oxidation.....	31
3. Photocatalytic-NO _x removal.....	32
3.1. Photo-selective catalytic reduction.....	32
3.1.1. Reduction mechanism in the presence of CO or hydrocarbons.....	32
3.1.2. Reduction mechanism in the presence of NH ₃	39
3.1.3. Photocatalysts for photo-SCR in the presence CO or hydrocarbons.....	39
3.1.4. Photocatalysts for photo-SCR in the presence of NH ₃	40
3.2. Photo-oxidation.....	40
3.2.1. Oxidation mechanism.....	40
3.2.2. Photocatalysts.....	41
3.2.3. Processes.....	42
3.3. Photo-decomposition.....	43
3.3.1. Decomposition mechanism.....	43
3.3.2. Photocatalysts.....	44
3.3.3. Processes.....	45
3.4. Section summary.....	45
4. Applications.....	45
4.1. Investigation of photocatalysts for real applications.....	46
4.2. Photo-deNO _x processes and materials applied in real applications.....	46

* Corresponding author. Tel.: +886 2 23631994; fax: +886 2 23623040.

E-mail address: cswu@ntu.edu.tw (J.C.S. Wu).

4.3.	Patents	47
4.3.1.	Materials	47
4.3.2.	Installations and applications	48
5.	Future trends and challenges in photo-deNO _x	48
5.1.	Proposed combination of photo-deNO _x with other primary or secondary methods	48
5.2.	The influence of water and oxygen in photo-SCR	49
6.	Summary and remarks	50
7.	Sources of further information	50
	Acknowledgements	50
	References	50

1. Introduction

Nitrogen(II) oxide and Nitrogen(IV) oxide, both considered NO_x, are very harmful and poisonous gases emitted primarily from combustion. Although these gases are also emitted from natural sources such as volcanic activity, forest fires, and atmospheric light, it is known that anthropogenic activities have made the largest contribution to total NO_x emission. The negative influence of human activity is irrefutable. The main anthropogenic sources of NO_x come from stationary power (mainly coal) plants and automobile engines [1–3]. During combustion, NO is created and can be subsequently oxidized in air to NO₂ in the overall Reaction (1.1).



NO_x negatively impacts the environment, human and animal health and plant vegetation. It creates environmental problems such as acid rain, photochemical smog, ozone layer depletion, Greenhouse effect (indirect impact), and ecological toxification [3–5]. Understanding the photochemical transformations of nitrogen oxides (NO, NO₂, NO₃) in urban air was recently reviewed by Sadanaga et al. [6]. It is believed that the increased NO_x and SO₂ have raised mortality, morbidity, hospital admissions, clinical symptoms, and lung function abnormalities in China over the last two decades [7]. Additionally, NO_x has also impacted indoor areas. For example, NO₂ levels were 3–5 times higher in residential areas relying heavily on gas for cooking in comparison to rural areas. Another problem is the interplay and interdependence of NO_x with other air pollutants, mainly volatile organic compounds (VOC). The co-created by-products (e.g., nitrous acid or peroxyacyl nitrate (PAN)) can be 10 times more toxic to humans than NO_x [8]. Commonly observed photolytic reactions are listed below:



where M represents a third molecule body (O₂, N₂) with significant contributions to photochemical smog. The presence of ozone in the troposphere can also damage the eyes and lungs [9]. Generally, NO_x causes respiratory illness and can increase the incidence of cancer. More specific information on the negative effects of NO and NO₂ on human health can be found in the literature [7–11].

The aim of this review is to present the current state of photocatalytic deNO_x processes. Another and undoubtedly important issue is photocatalytic methods for N₂O removal, but it is beyond the scope of this review. A recent publication by de Richter and Caillol surveys this topic [12]. The traditional thermal methods for NO_x abatement and NO_x generation (during combustion) are briefly presented as background.

1.1. Mechanism of NO generation

During combustion, NO can be created as a product of nitrogen oxidation in air (N₂) or nitrogen-containing fuel (fuel-N). Significant amounts of fuel-N are only found in solid and some liquid fuels

(e.g., coal or heavy oils). Transformation of fuel-N during combustion has already been described in the literature [13]. NO generation can be differentiated into two different processes: thermal and flame [14].

The thermal mechanism describes reactions that involve N₂, O₂, and heat. Zeldovich [15] proposed reactions for the formation of “thermal NO”.



The overall rate of NO formation is controlled by Reaction (1.4). The “Zeldovich Mechanism” described experimental data well at temperatures above 2000 °C. Wolfrum [16], Malte and Pratt [17], and Tomeczek and Gradoń [18,19] supplemented the original “Zeldovich Mechanism” by taking into account the influence of N₂O.



Tomeczek and Gradoń determined the rate coefficients of these three reactions and proposed the term “extended thermal mechanism” for both of Zeldovich’s reactions (Eqs. (1.4) and (1.5)) and the nitrous oxide reactions (Eqs. (1.6)–(1.8)) [18,19].

The flame mechanism describes the formation of NO in reactions that involve C, H, O and N compounds under rich and lean flame zones. A few “flame mechanisms” have been proposed in the literature:

- Fenimore mechanism (called also “prompt”) [20], with principal reaction



- NNH mechanism [21], with principal reaction



- NO formation via N₂O [18], with principal reaction



- Basic mechanism via NCN [22], with key reaction



It should be mentioned that “air-N” and “fuel-N” are not the same as “thermal” and “flame” mechanisms. The first terms describe the source of nitrogen introduced into the reaction zone, while the second terms describe the paths of NO formation. For example, during combustion of pure CH₄, both mechanisms (thermal and flame) exist. However, only “air-N” is introduced in this case. On the contrary, both “thermal” and “flame” mechanisms exist during coal combustion, and both “air-N” and “fuel-N” are oxidized to NO.

2. Methods for NO_x removal

Methods for NO removal can be divided into primary and secondary procedures [2]. The division of NO_x removal methods (including photo-processes) is shown in Fig. 1. The photo-deNO_x processes are classified as secondary procedure. Additionally, two new ideas for NO_x abatement have been proposed using the reduction of nitrogen oxides into harmless N₂ and the oxidation of NO_x into nitric acid.

2.1. Primary methods

Primary methods of NO_x removal are carried out inside a combustion zone (e.g., furnace) without the need for another reactor. In these methods, the combustion parameters are adjusted to reduce NO_x formation. Low-NO_x methods use various phenomena to influence NO_x formation. The design of low-NO_x primary technology has been focused on parameters influencing NO_x reduction. It is known that NO_x reduction can be enhanced by [14]:

- decreasing reactant residence time in high-temperature flame zones,
- creating reducing zones in the flame,
- decreasing oxygen concentration in the flame,
- reducing temperature peaks in the flame.

The primary methods that are based on these phenomena are:

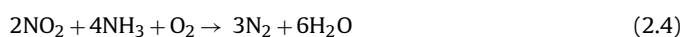
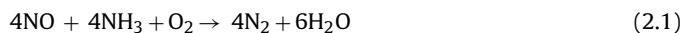
- fuel staging (reburning) [2], air staging (staging) [2],
- internal or external exhaust-gas recirculation (EGR, including low NO_x burners [2,14,23–26],
- FLOX and COSTAIR technologies [27,28], GAFT [29], and EGR applied in car engine systems [30,31]),
- precise control of excess air number (λ) [14,25,26,32],
- use of incombustible substances in the combustion zone [33,34].

2.2. Secondary methods

2.2.1. Reduction

The most common secondary methods are selective catalytic reduction (SCR) and selective non-catalytic reduction (SNCR) [3,35]. Examples of the other methods are absorption of NO_x, phase separation [2], NO_x storage and reduction (NSR) or ozone injection [3]. The main disadvantage of secondary measures is the need for additional equipment. However, these methods do not interfere with the combustion process and the deNO_x efficiency is generally higher compared to primary methods [2].

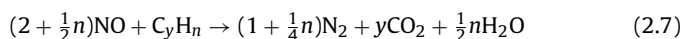
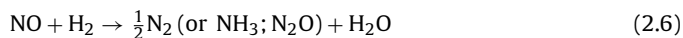
Selective catalytic reduction is realized by introducing NH₃, CO, H₂ or hydrocarbons and occurs on the catalyst surface. Usually, deNO_x processes are carried out at between 300 and 400 °C depending on the type of catalyst used. However, the process temperature can be decreased by combining SCR with non-thermal plasma treatment [36]. Types of catalysts and process conditions suitable for this method are described in the literature [2,3,35,37]. For ammonia, the main SCR reactions of NO_x are [35]:



Eqs. (2.1)–(2.4) describe the reduction of NO and NO₂ by NH₃ in the presence or absence of oxygen. Excess oxygen can cause decreased selectivity for N₂ formation and may influence the formation of N₂O or even cause the oxidation of ammonia into NO or NO₂. However,

oxygen plays an important role in the reduction of NO and NO₂. Eq. (2.1) is the preferred pathway if the proper stoichiometric ratio between NH₃, NO_x and O₂ can be maintained.

Oxygen is not the only component in exhaust gas, as SO₂, CO₂, and HCl can also be present. Unfortunately, these components also influence the consumption of NH₃ and the creation of corrosive products that may damage equipment. Some specific reactions for NO reduction are presented in the literature [35]. For CO, H₂ or hydrocarbons (C_yH_n), the overall NO reduction reactions are [35,38]:

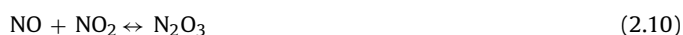


CO, H₂ and hydrocarbons are preferable to NH₃ for SCR because of the risk of ammonia leak. SCR is typically used in stationary combustion systems [2,3,35,37] and vehicle engine systems [30,38,39].

In general, Selective Non-Catalytic Reduction reactions are similar to SCR (Eqs. (2.1)–(2.4)), but are carried out without a catalyst. SNCR is realized by injecting active compounds (such as ammonia or urea) into a reactor placed behind a main combustion zone. High temperature is required (>800 °C) for this process, but excessively high temperature (>1000 °C) may cause ammonia to convert into NO_x [2,3]. The specific temperature window can be widened by simultaneously injecting other compounds (e.g., CO, CH₄, phenol, toluene) with the main reducing agent. The optimal reaction temperature can be lowered and the process efficiency enhanced using supporting compounds [40]. The efficiency of SNCR is lower than that of SCR under the same process conditions, and SNCR may encounter ammonia leaks more easily.

2.2.2. Oxidation

Removal of NO_x can be realized by absorption in water. The aim of this method is to eventually convert NO into HNO₃, but NO must first be oxidized into higher oxidation state nitrogen oxides. The main gas phase reactions are the following:



Further reactions are carried out in the liquid phase, and HNO₂ oxidation to HNO₃ is enhanced in the presence of ozone (in the liquid phase).



The presence of ozone is preferred because HNO₂ is unstable as a liquid and will transform into other species according to the following reaction:



Thus, the presence of ozone is recommended for increasing the absorption of NO_x [41]. This process can be carried out with simultaneous SO₂ absorption in euechlorine (a mixture of chlorine tetroxide and free chlorine) solution. Removal efficiencies of approximately 100% and 72% were achieved for SO₂ and NO_x, respectively, at 45 °C in a laboratory-scale scrubber [42].

NO_x can also be removed by phase separation. The boiling point of NO₂ at a pressure of 30 bar is approximately 100 °C. However, this process is not cost-effective because it requires complete conversion of NO into NO₂ (NO boiling point at 30 bar ≈ –100 °C). In addition, pressure strongly influences conversion rate. CO₂ (boiling point at 30 bar ≈ 0 °C) and NO₂ can be separated simultaneously, but the CO₂ condensate will likely be polluted with NO₂ [2].

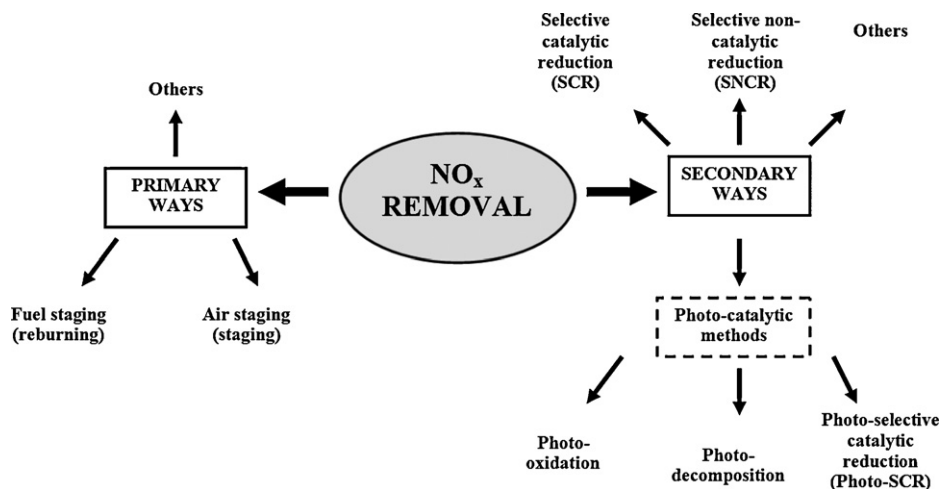


Fig. 1. The methods of NO_x removal.

NO can be oxidized by injecting ozone into exhaust gas. The NO oxidation rate is very fast in this method because O₃ decomposes into O₂ and a highly reactive O radical [43]. The created NO₂ can be subsequently reduced to N₂ by Na₂SO₃ or Na₂S. An example reaction of this process is shown below:



The deNO_x process can be carried out simultaneously with the de-SO₂ process. Using this combined process, 95% and 100% efficiencies were achieved for the removal of NO_x and SO₂, respectively [44].

3. Photocatalytic-NO_x removal

Photocatalysis is an innovative and promising technique for the removal of poisonous or undesirable compounds such as volatile organic compounds [45,46] or nitrogen oxides. This section is therefore focused on methods of photo-NO_x removal. NO removal by photocatalytic reactions is described, as are the types of photocatalysts used for these processes and the applications of photo-deNO_x reactions in real cases. Finally, the future of photo-deNO_x processes is also discussed.

Three methods for NO_x removal by photocatalysis have been presented in the literature: photo-decomposition, photo-oxidation and photo-SCR. These methods have advantages and disadvantages that will be described in detail in the following sections. Photo-decomposition and photo-SCR belong to reduction methods. The main aim of these deNO_x processes is thus transformation of this pollutant into N₂ and other harmless compounds. The photo-oxidation of NO_x will lead to nitric acid formation, which must be removed from the photocatalyst surface. The removal of NO by photocatalysis was first reported by Pichat et al. [47] and Courbon and Pichat [48]. They investigated not only NO decomposition on TiO₂ (Degussa P25) under UV light irradiation but also butanol oxidation using NO as oxidant (i.e., photo-SCR). The researchers observed transformation of NO into N₂ and N₂O. Later, Yokomichi et al. [49] proposed a photocatalyst based on zeolite Cu-ZSM-5 as an active material for NO_x decomposition. Many past studies attempted to develop or improve photocatalytic techniques increased NO_x removal efficiency.

In the following sections, the summary of photo-decomposition, photo-oxidation and photo-SCR are listed in Tables 1–3. The

efficiency of NO abatement (second column from the right in the tables) was calculated from the equation:

$$\text{Eff} = \left(1 - \frac{\text{NO}_{x\text{after}}}{\text{NO}_{x\text{before}}}\right) \times 100\% \quad (3.0)$$

where NO_{xbefore} represents the NO molar fraction measured before the photoreactor (inlet) and NO_{xafter} is the NO molar fraction measured in the outlet of the photoreactor.

3.1. Photo-selective catalytic reduction

Photo-selective catalytic reduction (photo-SCR) is a very attractive way to remove NO_x because it allows the transformation of pollutants into harmless gaseous compounds, such as N₂, without high temperatures. This process occurs on a photocatalyst surface and involves the reduction of NO_x in the presence of a reducing agent under light irradiation. NH₃ or hydrocarbons are typically selected as reducing agents, with the choice dependent on the process conditions. Photo-SCR by hydrocarbons or carbon monoxide is preferred because the use of NH₃ as a reducing agent can be risky due to secondary emission. In this case, an accurate material balance must be determined. Nevertheless, application of photo-SCR with hydrocarbons or CO in real scenarios is not easy. One of the major difficulties is the influence of water and oxygen, which will be discussed later. The oxidation of hydrocarbons into CO₂ must be considered. Another problem is that undesired compounds (e.g., N₂O) can appear as intermediate by-products. Fortunately, the reduction of N₂O photocatalytically is possible and examples have been described in the literature [50–53].

Table 1 summarizes photo-SCR and includes basic information such as photocatalyst used, conditions, and common reducing agents. The column “Max. eff. or selectivity” contains mainly deNO_x efficiency with selectivity appearing in brackets.

3.1.1. Reduction mechanism in the presence of CO or hydrocarbons

The mechanisms of photo-SCR are not well known and remain under intense investigation. Bowering et al. [58] proposed a mechanism for NO reduction on pure TiO₂ (Degussa P25) in the presence of CO. The main reactions occurring on the photocatalyst surface are:

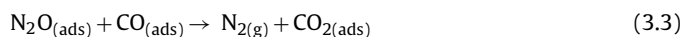


Table 1
Summary of NO_x photo-SCR processes.

Catalyst	Conditions		Main detected compounds	Main products	Max. eff. (or selectivity)	Reference
	(temperature, light, reactor, gas composition, stream rate ect.)	Reducing agent				
Hydrocarbon; CO photo-SCR TiO ₂ ("Hombifine N"; Sachtleben Chemie GmbH, Germany), 0.3–0.4 g, 357 m ² g ⁻¹	21–150 °C UV (66.8 mW/m ² 43.2–56.8% vis–UV), 2000 ppm hydrocarbon/2000 ppm NO/12% O ₂ /He 250 ml/min	ethane, ethene, propane, propene, <i>n</i> -butane carbon monoxide	NO, N ₂ O, NO ₂ , hydrocarbon, CO ₂	N ₂ , NO ₂ , N ₂ O	100	[54]
Pd ion-substituted TiO ₂ (Ti _{1-x} Pd _x O _{2-xδ}), or Pd/TiO ₂ (imp) (from titanium isopropoxide TiO(i-pr) ₄ and PdCl ₂) 0.15 g, 50 m ² g ⁻¹ . Ag/TiO ₂ ; (Degussa P25, AgNO ₃)	35 °C, UV (125 W medium-pressure mercury lamp, 3.5 eV with corresponding photon flux of 6 × 10 ⁻⁶ mol of photon cm ⁻² s ⁻¹), continuous flow 5000 ppm NO/5000 ppm CO/He, 20 ml/min. UV (400 W medium pressure mercury lamp), continuous flow, 909 ppm NO/1818 ppm CO/Ar 5.5 ml/min	carbon monoxide	NO, N ₂ O, N ₂ , CO ₂ , O ₂	N ₂ , N ₂ O	100	[55,56]
Degussa P25	UV (400 W medium pressure mercury lamp), continuous flow, 909 ppm NO/1818 ppm CO/Ar 5.5 ml/min	carbon monoxide	NO, N ₂ O, N ₂	N ₂ O, N ₂	53 (select. N ₂ 90–100%) 100% (select. N ₂ 65%)	[57] [58]
Vanadium silicalite-1(VS-1) (Si/V = 120) (from tetraethyl-orthosilicate and VOSO ₄ ·3H ₂ O)	25 °C, UV high pressure mercury lamp with color (λ > 270 nm) or water filters, in situ, spectroscopic measurements, Propane: 1.97·10 ⁻⁴ mol/g-cat, NO: 1.82·10 ⁻⁴ mol/g-cat	propane	N ₂ , N ₂ O, O ₂ also C ₃ H ₆ , C ₂ H ₄ , CH ₃ CHO and CO ₂	N ₂ , N ₂ O, O ₂ also C ₃ H ₆ , C ₂ H ₄ , CH ₃ CHO and CO ₂		[59]
TiO ₂ /PdO or TiO ₂ /Pd (Degussa P25, Pd(NO ₃) ₂), 0.5 g	Room temp, UV 100 W high pressure Hg lamp with 320–500 nm filter (Exfo Acticure 4000), continuous flow, 400 ppm NO/5000 ppm C ₃ H ₈ /5% O ₂ , 5 ml/min (total), GHSV = 343 h ⁻¹	propane	NO, N ₂ O, NO ₂	N ₂	94% for Pd load. 60% for PdO load.	[60]
Ru, Rh, Cu, Ru-Rh, or Ru-Cu supported on TiO ₂ (P25, RuCl ₃ ·hydrate, RhCl ₃ ·hydrate, CuCl ₂ , Fluka), 100 or 200 mg The Corning cordierite monolith (2Al ₂ O ₃ 5SiO ₂ 2MgO, 30% porosity) coated by PtO _x PdO _y /TiO ₂	52 °C, solar simulator (Hanau, Suntest, 80 mW/cm ² total output, λ < 390 nm, Batch reactor 7.5% NO/12.5% CO/80% He	carbon monoxide	CO, N ₂ , NO, CO ₂ , N ₂ O,	N ₂ O, CO ₂		[61]
TiO ₂ /PdO (Degussa P25, Pd(NO ₃) ₂), 0.037 g	21–120 °C, the Exfo S1500 (USA) high-pressure Hg lamp (46.9 mW/cm ² , filter 320–500 nm), continuous flow reactor (monolith with optical fibers inside the reactor channels), 400 ppmv NO in N ₂ , 5000 ppmv C ₃ H ₈ in N ₂ , 5 vol% O ₂ in He, H ₂ O introduced by a saturator, compounds molar ratio: NO:C ₃ H ₈ = 1:24, NO:C ₃ H ₈ :O ₂ = 1:24:120, NO:C ₃ H ₈ :H ₂ O = 1:24:41 7 ml/min, GHSV = 3.2 h ⁻¹	propane	NO, N ₂ O, NO ₂ , H-Cs	N ₂	90	[62]
TiO ₂ /PdO (Degussa P25, Pd(NO ₃) ₂), 0.037 g	30–120 °C, the Exfo S1500 (USA) high-pressure Hg lamp (200 mW/cm ² , filter 320–500 nm), continuous flow, 400 ppm NO/5000 ppm C ₃ H ₈ /5% O ₂ , 0.55–1.6 v.H ₂ O 10 ml/min (total), GHSV = 330–1090 h ⁻¹	propane	NO, NO ₂	N ₂	94	[63]
NH ₃ photo-SCR TiO ₂ (Super Titania F-6; SHOWA DENKO) + 10% _{max} WO ₃ (aqueous solutions of ammonium tungstate parapentahydrate; wet impregnation followed by evaporation to dryness)	Room temp, PERKIN-ELMER PE300BF 300 W Xe lamp; fixed bed flow reactor, 1000 ppm NH ₃ /1000 ppm NO/O ₂ 2%/Ar bal.	NH ₃	N ₂ , N ₂ O	N ₂	79%	[64]
TiO ₂ (Super Titania F-6 (Lot No.H04320); SHOWA DENKO) loaded by metals 1% (V ₂ O ₅ , CrO ₆ , MnO, Fe ₂ O ₃ , CoO, NiO, CuO, ZnO, Y ₂ O ₃ , ZrO ₂ , Nb ₂ O ₅ , MoO ₃ , Ta ₂ O ₃ , WO ₃)	Room temp PERKIN-ELMER PE300BF 300 W Xe lamp. fixed bed flow reactor, 1000 ppm NH ₃ /1000 ppm NO/O ₂ 2%/Ar bal, GHSV = 50,000 h ⁻¹	NH ₃	N ₂ , N ₂ O	N ₂	Min. 12.1%, max. 63.4%	[65]
TiO ₂ (Japan Catalysis Society; (JRC-TIO-1, 2, 3, 4, 5), Ishihara; Sangyo Kaisha Ltd. (ST-01, 21, 30L, 31, 41); TAYCA Co. (TKP-101, 103)), 0.6–1.14 g	Room temp., 300 W ultra-high Xe lamp (Perkin-Elmer), Fixed bed flow reactor, 1000 ppm NO/1000 ppm NH ₃ /2–10% O ₂ /Ar bal., 100 ml/min or 250–1250 ppm NO/250–1250 ppm NH ₃ /0.5–3.5% O ₂ , GHSV = 4000–16,000 h ⁻¹	NH ₃	N ₂ , N ₂ O	N ₂ , N ₂ O	73%	[66]
TiO ₂ /Si (doping, 1–10%), hydrothermal method (Ti(OC ₄ H ₉) ₄ : (C ₂ H ₅) ₄ SiO ₄), 5 g ± 10%	50 °C, 250 Whigh-pressure Hg lamps (Philips). From 300 to 400 nm maximum light intensity at 365 nm, Continuous flow, 400 ppm NO/400 ppm NH ₃ /3% O ₂ /bal N ₂ 2000 ml/min reactor, GHSV = 600 h ⁻¹	NH ₃	–		60%	[67]
Pressed wafers of TiO ₂ (Cab-o-Ti, Cabot Corp., 85% anatase, 15% rutile, surface area 50 m ² g ⁻¹), 50 ± 5 mg, 20 mm × 10 mm	30–100 °C, Near UV 100 W mercury lamp with filters: heat absorbent glass filter (Schott KG1), black glass filter (Schott UG1) 365 nm, ≈40 mW/cm ² , Batch reactor, 10 Torr of NH ₃ and 10 Torr of NO	NH ₃	N ₂ , O ₂ , N ₂ O	N ₂ , N ₂ O		[68]

Table 2
Summary of NO_x photo-oxidation process.

Catalyst	Conditions (temperature, light, reactor, gas composition, stream rate ect.)	Main detected compounds	Main products	Max. eff. or selectivity	Ref
TiO ₂ (anatase aqueous sol; Ishihara Sangyo Kaisha Ltd., STS-21, 20 nm particle diameter)	Room temp., UV black fluorescent lamp (Toshiba Co., FL10BLB-A; wavelength, 300–400 nm; UV, 2 mW/cm ²), 1 ppmNO/N ₂ with wet or dry air, 2 l/min	NO, NO ₂ , NO ₃	NO ₂ , HNO ₃	~20%	[74]
Anatase, brookite and rutile type nitrogen-doped (TiO _{2-x} N _y) Homogeneous Precipitation–Solvothetmal Process' (HPSP) in TiCl ₃ –hexamethylenetetramine (C ₆ H ₁₂ N ₄) aqueous and alcohol solutions	450 W high-pressure mercury Lamp >510 nm, >400 nm, and >290 nm, 1 ppm NO/50% air/N ₂ , 200 ml/min, GHSV = 32 h ⁻¹	NO, NO ₂	(not clear)	~39% (λ > 510 nm); ~50% (λ > 400 nm); ~84% (λ > 290 nm)	[75]
TiO ₂ /Pt (0.42–0.47%); (TiO ₂ , H ₂ PtCl ₆), 4 g	“black” light (Matsushita Electric Model FL20SBL-B); “white” light (Toshiba Model FL20SS-W) L42 filter (Asahi Techno Glass λ > 420 nm, 3 mW/cm ² for UV 5700 lx for vis 3 ppm NO/humid air, continuous flow reactor, 3 l/min	NO, NO ₂	HNO ₃	~82% (UV) ~68% (vis)	[76]
Commercial concrete paving stones containing TiO ₂ , 49.5 ± 0.5 mm width, 99.5 ± 0.5 mm length, 200 mm height	3 fluorescent tubes (Philips CLEO Compact, 25 W, λ _{max} = 345 nm), 10 W/m ² , 0.1; 0.3; 0.5 or 1 ppmv NO/synthetic air (20.5% O ₂ , 79.5% N ₂) humid conditions RH = 50%, laminar flow reactor (Re ≈ 65), 3 l/min, GHSV = 7035 h ⁻¹	NO, NO ₂	NO ₂ , HNO ₂ , HNO ₃	90.6%	[77,78]
Degussa P25 or TiO ₂ /Al ₂ O ₃ (sol–gel from Al(C ₃ H ₇ O) ₃ and Ti(C ₃ H ₇ O) ₄), 0.2 g	two compact 26 W black lights (Camelion, LH26-30) 45–50 ppm NO, 7 vol.% O ₂ and bal. N ₂ , 440 ml/min	NO, NO ₂	NO ₂	~30% (at steady st. cond.)	[79]
Ultrafine powdered TiO ₂ catalysts (grain size, 0.02–1 μm, Catalysis Society of Japan, JRC-TiO-2, -3, -4, and -5)	Toshiba SHL-100UV high-pressure Hg lamp, 10 ppm NO, 5–17% O ₂ , N ₂ , Flow reactor, GHSV = 400 h ⁻¹	NO, N ₂ , O ₂ , N ₂ O	NO ₂	~50%	[80]
Pd-modified TiO ₂ (TiO ₂ Degussa P25, Wet Impregnation (Pd ²⁺ /HCl solution), Neutralization (Pd ²⁺ /HCl solution), Photo-deposition (PdCl ₂ in methanol)	80 ± 5 °C, Hg-arc lamp (125 W, Philips) 300–400 nm with the maximum light intensity at 365 nm, 100 ppm NO, 21%O ₂ , N ₂ , air humid conditions, 2 l/min, continuous flow, GHSV = 360 h ⁻¹	NO, NO ₂	NO ₂ , HNO ₂ NO ₃ ⁻	85%	[81–83]
Ultrafine particie (7; 20; 200 nm) TiO ₂ (ST-series, Ishihara Techno Corp.), 0.5 g	UV (FL15BL, 2 × 15 W, TOSHIBA), 0.40–0.90 mW/cm ² , 100 ppm NO _x , air from compressor two-dimensional fluidized bed reactor 24.3 cm/s → 0.55 ml min, GHSV = 1930 h ⁻¹	NO, NO ₂	HNO ₃	Non steady-state cond. ~90–10%	[84]
TiO _{2-x} N _y , TiO _{2-x} N _y /Fe, TiO _{2-x} N _y /Pt (anatase TiO ₂ powder (ST-01, Ishihara Sangyo Kaisha, Osaka, Japan), NH ₃ , Fe(NO ₃) ₃ (Wako Pure Chemical Industries Ltd., Osaka, Japan), Pt(NH ₃) ₂ (NO ₃) ₂ (Tanaka Kikinzoku Kogyo K.K., Tokyo)), 1.2 g	25 °C, LED light (red–630 nm, green–530 nm, blue–470 nm, UV–375 nm), 1 ppm NO-50 vol.% air/N ₂ (bal.), 200 ml/min, GHSV = 32 h ⁻¹	O ₂ NO	HNO ₂ , HNO ₃	17% (red light), 27% (green), 37% (blue) 38% (UV)	[85]
TiO _{2-x} N _y , (Degussa P25, hexamethylenetetramine–C ₆ H ₁₂ N ₄ , ammonium carbonate (Kanto Chem. Japan), urea)	Vis and UV (450 W high-pressure mercury lamp with filters <290, <400, and <510 nm), 1 ppmNO/N ₂ with air (1:1), 200 ml/min, GHSV = 32 h ⁻¹	NO		~60% (λ > 290 nm), ~42% (λ > 400), ~38% (λ > 510 nm)	[86]
PtO _x -doped TiO ₂ and PtO _x -loaded TiO ₂ (TiO ₂ , Hombikat UV100 (Sachtleben Chemie, 100% anatase) and the other was synthesized by acid-catalyzed sol–gel process, Pt(NH ₃) ₄ (NO ₃) ₂ or H ₂ Pt(OH) ₆), 0.5 g	Black light lamp (330–420 nm), visible light LED (blue, 430–530 nm), (green, 470–570 nm), (red 590–680 nm), 1 ppmNO/N ₂ /air (humidified or dry), continuous flow 1 l/min	NO, NO ₂	HNO ₂ , NO ₂ HNO ₃	~62% (UV), ~52% (blue), ~48% (green), ~34% (red)	[87]
C-doped TiO ₂ (tetrabutyl orthotitanate) 0.5 g	LED Vis (465; 515; 640 nm) and UV (365 nm), 1 ppm NO/N ₂ /air (humidified), continuous flow 1 l/min, GHSV = 108 h ⁻¹	NO, NO ₂	HNO ₃ , HNO ₂	(for NO) ~88% (UV), ~88% (blue), ~86% (green), ~78% (red)	[88]
Pt/TiO ₂ , Rh/TiO ₂ (H ₂ PtCl ₆ /TiO ₂ , RhCl ₃)	Blue fluorescent lamp (10 W, S-3410, Sudo, maximum energy at 450 nm), black light (10 W, FL-10BL, Hitachi, maximum UV energy at 369 nm) 10 ppm NO/air, continuous flow, 110 ml/min	NO, NO ₂	NO ₂ , and NO ₃ ⁻		[89]

Commercial TiO ₂ (May and Baker laboratory chemicals, purity > 98%)	UV, 4 × 60 W strip tubes, (Radio Spares, model No. 556-238, λ=320 nm), 109 ± 5 ppm NO, 21.0 ± 0.4% O ₂ , N ₂ ball. (dry or wet cond.) continuous flow		(XPS) and Raman spectroscopy are used to study the surface reaction between the nitrogen oxides and the TiO ₂ surface.		[90]
TiO ₂ (anatase, 0.15 μm, surface area: 21 m ² g ⁻¹ , Shinshu Ceramics, Japan), 4 g hydroxyapatite (Ca ₁₀ (PO ₄) ₆ (OH) ₂ , 9.2 μm, surface area: 59 m ² g ⁻¹ , Shinshu Ceramics, Japan), 4 g	UV, black light (λ = 300–400 nm, FL8BL, 8 W, NEC, Japan), Annular diffusion scrubber coated with a mixture of titanium dioxide (TiO ₂) and hydroxyapatite (Ca ₁₀ (PO ₄) ₆ (OH) ₂), 100–450 ppbv of NO and/or NO ₂ in the air, humid cond. 21–78%, continuous flow 0.2–5.0 l/min, GHSV = 1005–5030 h ⁻¹	NO, NO ₂ , NO ₃ ⁻ , NO ₂ ⁻ ,	NO ₂ , HNO ₃	~100% (time 15 min, flow rate 1 l/min, humid conditions)	[91]
Mixture of TiO ₂ (Degussa P25, particle 20 nm and Kokusan Kagaku Co, anatase), and activated carbon, also Fe ₂ O ₃ or ZnO, 200–250 mg	~35 °C, cylindrical bank of 12 black lights (λ = 300–400 nm), 1 ppm NO _x in purified air or O ₂ –N ₂ mix., humidity to 72%, continuous flow 500 ml/min, GHSV = 37500 h ⁻¹	NO, NO ₂ , NO ₃ ⁻	HNO ₃ , NO ₂	The best efficiency for TiO ₂ -AC-Fe ₂ O ₃ mixture	[92]
Commercial and plasma treated TiO ₂ (Ishihara Sangyo Kaisha, 100% anatase, crystallite size of 7 nm, nominal specific surface area of 300 m ² g ⁻¹) 0.2 g	Room temp., 300 W xenon lamp Visible light (up to 600 nm) without a decrease in the ultraviolet light activity, 1 ppm NO in dry, purified air, continuous flow 1500 ml/min, atm. pressure, GHSV = 180 h ⁻¹	NO, NO ₂	NO ₃ ⁻	~13% for vis., ~20% for UV-A	[93]
TiO ₂ (Degussa P25) coated on a glass fiber filter (Whatman) 1.64 g ± 5% of TiO ₂	6 W UV lamp (Cole-Parmler), 365 nm, 0–900 ppb NO/0–70 ppb BTEX (mixture of benzene, toluene, ethylbenzene and o-xylene)/humid air (2100–22000 ppmv H ₂ O), continuous flow ~5 l/min, GHSV = 5.3 h ⁻¹	NO, NO ₂ and VOCs (BTEX)	NO ₂	Over 90%	[94]
TiO ₂ loaded on activated carbon (1.64 g ± 5% of TiO ₂)	6 W UV lamp (Cole-Parmler), 365 nm, 200 ppb NO/20 ppb BTEX (mixture of benzene, toluene, ethylbenzene and o-xylene)/humid air (2100– 22000 ppmv H ₂ O), continuous flow, GHSV = 16–98 h ⁻¹	NO, NO ₂ and VOCs (BTEX)		66%	[95]
TiO ₂ (Degussa P25)	15 W daylight/UV lamp (30% UVA and 4% UVB), NO _x mixture prepared in-situ, 1–2 ppm, continuous flow 0.6 l/min, GHSV = 7.2 h ⁻¹	NO, NO ₂		35% NO, 20% NO _x	[96,97]
TiO ₂ (Degussa P25)	two 8 or 25 W black lights (GE, F8T5-BL or F25T8-BL), 5–60 ppm/0–20% O ₂ /N ₂ relative humidity 0 to 75%, GHSV = 150–1800 h ⁻¹	NO, NO ₂		80% NO _x	[98]
TiO ₂ (Degussa P25), 5 g	80 ± 5 °C, Hg-arc lamp (125 W, Philips), 20–168 ppm NO/air/N ₂ , relative humidity 8–100%, GHSV = 120–720 h ⁻¹	NO, NO ₂ , O ₂		27%	[99]
TiO ₂ and TiO ₂ -10 wt.% Al. (high-velocity oxygen fuel (HVOF) spraying)	UV (360 and 380 nm)			25–42% for NO and 14–18% for NO _x	[100]
TiO ₂ coatings elaborated by various thermal spraying methods (plasma spraying in atmospheric conditions, suspension plasma spraying, and high-velocity oxyfuel spraying), 0.4 g	15 W daylight/UV lamp (30% UVA and 4% UVB), NO _x mixture prepared in situ, 1–2 ppm, continuous flow 0.6 l/min	NO, NO ₂		52% for NO 34% for NO _x	[101]
TiO ₂ nanopowder coatings (ST-01, Ishihara Sangyo, Japan, pure anatase, coatings prepared by plasma spraying from an agglomerated nanopowder and liquid suspension plasma spraying)	15 W daylight/UV lamp (30% UVA and 4% UVB), NO _x mixture prepared in-situ, 1–2 ppm, continuous flow 0.6 l/min, GHSV = 7.2 h ⁻¹	NO, NO ₂		~50% for NO, ~30% for NO _x	[102]
TiO ₂ coatings (anatase form: Ishihara Sangyo, Japan, Millennium Inorganic Chemicals, France and Degussa P25 thermal spraying: atmospheric plasma spraying (APS), suspension plasma spraying (SPS), and high-velocity oxygen fuel spray process (HVOF)	15 W daylight/UV lamp (30% UVA and 4% UVB), NO _x mixture prepared in situ, 1–2 ppm, continuous flow 0.6 l/min	NO, NO ₂		52% for NO 34% for NO _x	[103]
The HyCOM TiO ₂ (from titanium tetrabutoxide in toluene) mechanically mixed with A or Y form zeolite; 0.12 g	UV black lamp, 10 ppm NO in air, fixed bed continuous flow reactor, 110 ml/min	NO, NO ₂ , N ₂	NO ₂	96% for NO _x	[104]

Table 2 (Continued)

Catalyst	Conditions (temperature, light, reactor, gas composition, stream rate ect.)	Main detected compounds	Main products	Max. eff. or selectivity	Ref
Carbon-doped TiO ₂ (Kronos, Germany) as covered layer on glass fibers, sprayed onto wool fabric	Three cool day light lamps of each 25 W (Philips, the Netherlands, 400–700 nm, 1–13 W/m ²) 0.1–1 ppm NO in synthetic air (20.5% O ₂ , 79.5% N ₂) RH 10–70%, continuous flow, 1–5 l/min, GHSV = 2000–6000 h ⁻¹	NO, NO ₂	NO ₂	~20%	[105]
N-doped TiO ₂ nanoparticles (from titanium (IV) isopropoxide, triethylamine as nitrogen source; sol-gel) on glass support	Room temp., 300 W solar lamp (Radium Sanolux HRC 300–280; λ = 380–600 nm), 500 ppb NO _x in air/N ₂ mixture, RH 50%, batch reactor	NO _x (NO + NO ₂)	NO ₂ , HNO ₂ , HNO ₃		[106]
TiO ₂ -MCM-41 (alcoholic solution of Ti(iOPr) ₄ incipient wetness impregnation), 50 mg	Room temp., UV mercury vapour lamp, spectral range 315–400 nm, power, 125 W; Helios Italquartz, GN125RZS, 8.50 W/m ² , 100 ppb NO in air, 2780 ml/min fixed-bed reactor	NO, NO ₂	NO ₂ , NO ₃ ⁻	60%	[107]
Mn-doped amorphous TiO ₂ containing 0.1% and 1% Mn (w/w), 30 g	23 °C, visible light (OSRAM UltraVitalux 300 W lamp to simulate solar light irradiation and Philips TL-D Super80 18W-840 lamp to simulate indoor-light irradiation), the photocatalyst powder was spread homogeneously in a 0.1 m radius Petri dish and placed in a 0.45 m ³ environmental test chamber, 200 ppbv NO in air (relative humidity 50%)	NO, NO _x	HNO ₃	95% after 6 h of irradiation	[108]
TiO ₂ nanoparticles (commercial slurry containing anatase-TiO ₂ , Evonik) incorporated in a polymer-matrix-based coatings (acrylic binder, Hexion D2040).	Room temp., 300 W OSRAM Ultravitalux bulb (close to daylight), measured UV-A 5.8 w/m ² , flow reactor (d. 60 mm, l. 300 mm). The coatings were applied to construction materials such as mortars, glass plates and non-adsorbent cardboard material (control samples 100 mm × 50 mm), 400–2000 ppb of NO in air (relative humidity 0–74% at 25 °C), 1.5 l/min, GHSV = 318 h ⁻¹	NO, NO ₂ , NO ₃ ⁻ , NO ₂ ⁻	NO ₂ , NO ₃ ⁻	52%	[109]
Pure TiO ₂ , B-doped TiO ₂ , N-doped TiO ₂ , B, N-codoped TiO ₂ (precursors: TiCl ₄ , H ₃ BO ₃ , urea; aerosol-assisted flow synthetic method) 0.2 g	Room temp., Visible and simulated solar light (300 W commercial tungsten halogen lamp (General Electric) with UV filter (200–420 nm)), rectangular flow reactor, 400 ppbv NO in air (relative humidity 70%), 4 l/min, GHSV = 53 h ⁻¹	NO	HNO ₂ , HNO ₃	53%	[110]
carbon-containing (anhydrous ethanol as carbon source) nano-structured TiO ₂ (Ishihara ST01) 10 g	Room temp., UV (black lamp 352 nm) and visible (LED 465 and 515 nm) light, continuous flow reactor, 1 ppmv NO in air (relative humidity 50%), 1 l/min, GHSV = 190 h ⁻¹	NO, NO ₂	HNO ₂ , HNO ₃ , NO ₂	44%	[111]

Table 3
Summary of NO_x photo-decomposition process.

Catalyst	Conditions (temperature, light, reactor, gas composition, stream rate ect.)	Main detected compounds	Main products	Max. eff. or selectivity	Ref.
TiO ₂ (ionized cluster beam method) Cr- or V-ion-implanted	2 °C, Vis 100 W high-pressure Hg lamp (Toshiba SHL-100UVQ-2) with a filter ($\lambda > 450$ nm), batch reactor (12.3 mol NO) 12.3 mol of NO in 30 ml cell, batch reactor	N ₂ , O ₂ , N ₂ O	N ₂ , O ₂ , N ₂ O		[121]
TiO ₂ (the Catalysis Society of Japan JRC-TIO-4) Cr- or V-ion-implanted (high-voltage acceleration technique)	22 °C UV and Vis; high-pressure Hg lamp (Toshiba SHL-100UV) $\lambda > 450$ nm and $\lambda < 380$ nm,	N ₂ , O ₂ , N ₂ O	N ₂ O N ₂ , O ₂ ,		[122]
Ion exchanged Cu ⁺ /ZSM-5 and Ag ⁺ /ZSM-5 zeolite	25 °C, 2 Torr NO (for Cu ⁺ catalyst), 10 torr NO (for Ag ⁺ catalyst) UV ($\lambda > 250$ nm)	N ₂ , O ₂ , N ₂ O, NO ₂	N ₂ , O ₂ (N ₂ O, NO ₂ negligible) for Cu ⁺ , N ₂ , N ₂ O NO ₂ for Ag ⁺	Ag ⁺ catalyst is 10 times high eff. than Cu ⁺	[123]
Cu ⁺ dispersed in SiO ₂ (Cu(NO ₃) ₂ × 3H ₂ O, sol-gel process and the reduction treatment with H ₂)	2 °C Toshiba mercury lamp (SHLS-1002B) ($\lambda > 280$ nm)		N ₂ , O ₂		[124]
TiO ₂ Degussa P25 0.12 g TiO ₂ /g SiO ₂ (bed support), (also without irradiation at temperature range 50–350 °C)	40 °C, UV black light lamps (4 × 8 W, Sankyo Denki, Japan, F8T8 $\lambda_{\text{max}} = 365$ nm) white light (4 × 8 W, Sankyo Denki, Japan, G8T8 $\lambda_{\text{max}} = 254$ nm) 0–4 mW/cm ² annular flow-type and two-dimensional fluidized-bed photoreactors; 50–138 ppmv NO/He, 200 ml/min, GHSV = 160–1265 h ⁻¹	NO, NO ₂ , N ₂ O, N ₂ , O ₂	N ₂ , O ₂	>70%	[125]
Ag ⁺ /ZSM-5 zeolite ((SiO ₂ :Al ₂ O ₃ mole ratio=23:1, TOSOH, Ag(NH ₃) ₂ ⁺ -solution, ion-exchange method)	25 °C, high pressure mercury lamp with a water filter ($\lambda > 250$ nm), 10 Torr of NO	N ₂ , N ₂ O, NO ₂	N ₂ , N ₂ O, NO ₂		[126]
Vanadium silicalite (VS-2) and Ag ⁺ /ZSM-5 (tetraethylorthosilicate VCl ₃ × nH ₂ O or VOSO ₄ × nH ₂ O hydrothermal synthesis; Ag(NH ₃) ₂ ⁺ , SiO ₂ /Al ₂ O ₃ = 23.3 ion-exchange methods)	22 °C, high pressure mercury lamp with filter ($\lambda > 280$ nm and $\lambda > 250$ nm), 10 Torr of NO and additionally O ₂ and H ₂ O (20%)	N ₂ , N ₂ O, NO ₂ ,	N ₂ , N ₂ O, O ₂ (for VS-2) N ₂ , N ₂ O, NO ₂ (for Ag ⁺ /ZSM-5)		[127]
Titanium oxides (TiO ₂ JRC-TIO-4: anatase 92%, rutile 8%, Catalysis Society of Japan) with zeolites as supportes with different Si/Al ratios, ion-exchange and impregnation method (Ex.Ti/Y(x) (Si/Al) 5.6, 13.9 and 390; ex.Ti/ZSM-5, imp. Ti/ZSM-5 zeolities, TOSOH corporation, 100 mg,	22 °C, 75 W high-pressure Hg lamp ($\lambda > 280$ nm); Reactor: quartz cell with a flat bottom (60 ml) connected to a conventional vacuum system (10–6 Torr range), 7.8 μ mol of NO	N ₂ , O ₂ , N ₂ O, NO ₂	N ₂ , O ₂ , N ₂ O	max N ₂ (selectiv.) 88%	[128]
Mesoporous Ti-HMS catalyst (Tetraethyl orthosilicate (TEOS), tetraisopropyl orthotitanate (TIPOT), and a long-chain alkylamine surfactant (dodecylamine, DDA) as the source for the silica, titanium, and template, respectively), 100 mg (or 1 g for flow reactor) TiO ₂ (P-25) as a reference	22 °C, 75 W high-pressure Hg lamp ($\lambda > 280$ nm), continuous flow and closed reactor, Reactor: quartz cell with a flat bottom (60 ml) connected to a conventional vacuum system (10–6 Torr range), 25 ml/min, 7.8 μ mol of NO or 25 mL/min 10 ppm NO/He, GHSV = 25 h ⁻¹	N ₂ , O ₂ , N ₂ O, NO	N ₂ , O ₂ , N ₂ O	~25% (for flow system)	[129]
Transition metal oxides (Ti, V, Mo, Cr, etc.) incorporated within the framework of zeolites, especially Ti-oxide/Y-zeolite (SiO ₂ /Al ₂ O ₃ = 5.5; 1.1 wt.% as TiO ₂), Mo-MCM-41 and Cr-HMS (UV, sunlight or vis light)	22 °C, UV or vis light ($\lambda > 420$ nm for V ion-implanted Ti-HMS and Ti-MCM-41 catalysts), NO with and without propane and also with CO	N ₂ , O ₂ , N ₂ O, NO ₂ ⁻	N ₂ , O ₂ , N ₂ O	97% N ₂ selectiv., eff. with propane is approximately 5 times higher	[69]
Mesoporous Ti-MCM-41 (Ti 0.15; 0.6; 0.85; 2.00 wt%) (tetraethyl orthosilicate and tetraisopropyl orthotitanate and cetyltrimethylammonium bromide as the template)	22 °C, 100 W Hg lamp ($\lambda > 240$ nm)	N ₂ , O ₂ , N ₂ O, NO ₂ ⁻	N ₂ , O ₂ , N ₂ O		[130]
Cr or V ion-implanted TiO ₂ (the Catalysis Society of Japan, JRC-TIO-4)	2 °C, high pressure Hg lamp (Toshiba SHL-100UV, $\lambda > 450$ nm as visible light and $\lambda \sim 380$ nm as UV light), batch reactor, 12.8 μ mol NO	N ₂ , O ₂ , N ₂ O	N ₂ , O ₂ , N ₂ O		[131]
V, Cr, Mn, Fe, Ni ion-implanted TiO ₂	2–22 °C, high pressure Hg lamp (Toshiba SHL-100UV, $\lambda > 450$ nm as visible light and $\lambda \sim 380$ nm as UV light), or outdoor solar light, good photo-actvity for $\lambda > 550$ nm and for UV batch reactor		N ₂ , O ₂ , N ₂ O	effectiveness V > Cr > Mn > Fe > Ni good photo-actvity for $\lambda > 550$ nm and for UV	[132]

Table 3 (Continued)

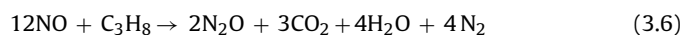
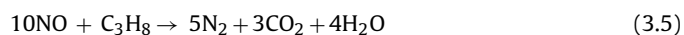
Catalyst	Conditions (temperature, light, reactor, gas composition, stream rate ect.)	Main detected compounds	Main products	Max. eff. or selectivity	Ref.
Cr or V ion-implanted TiO ₂ (the Catalysis Society of Japan, JRC-TIO-4)	22 °C, high pressure Hg lamp (Toshiba SHL-100UV, λ > 450 nm as visible light and λ ~ 380 nm as UV light), or outdoor solar light 38.5 mW/cm ² batch reactor		N ₂ , O ₂ , N ₂ O		[122]
Cr or V ion-implanted TiO ₂ (the Catalysis Society of Japan, JRC-TIO-4), 3.6 g Also soundproof highway walls coated with titanium oxide photocatalysts for the elimination of NO _x	high pressure Hg lamp (Toshiba SHL-100UV, λ > 450 nm as visible light and λ ~ 380 nm as UV light), or outdoor solar light 38.5 mW/cm ² batch reactor, also for 400–600 nm. Continuous flow or batch reactor, 18 l/min				[133]
metal ion-implantation TiO ₂ catalyst, Ti/zeolite or these un-implanted photocatalysts (highly dispersed tetrahedrally coordinated Ti-oxide species constructed within the zeolite frameworks, compared with bulk semiconducting TiO ₂ , UV or vis light resp. Ti/Beta(OH) zeolite, Ti/Beta(F) zeolite, Ti/HMS, Ti/MCM-41) REVIEW	UV light, visible light, solar light	N ₂ , O ₂ , N ₂ O	N ₂ , O ₂ , N ₂ O	~93% N ₂ selectivity	[119]
Anatase TiO ₂ , with a large surface area and numerous OH groups (the Catalysis Society of Japan, JRC-TIO-2, -3, -4, and -5, grain size, 0.02–1 μm), 150 mg	25 °C and higher, Toshiba SHL-100UV high-pressure Hg lamp with filter (λ > 270 nm) large-scale flow reaction system, 10 ppm NO/He, and also + (4.8–17%vol) O ₂ 100 ml/min, GHSV = 400 h ⁻¹	N ₂ , O ₂ , N ₂ O	N ₂ , O ₂ , N ₂ O	11% Eff. grad. JRC-TIO-4 > -3 > 5 > 2, the highest eff. at room temp.,	[80]
Vanadium silicalite (VS-2),	22 °C, UV high-pressure mercury lamp through water and color filters (λ > 280 nm), batch quartz reactor, NO pressure (2–13) Torr	N ₂ , O ₂ , N ₂ O	N ₂ , O ₂ , N ₂ O		[134]
Cu ⁺ /ZSM-5 (copper: aqueous (Cu(NH ₃) ₄) ²⁺ 0.1–2.3 Cu wt%; zeolite; Si/Al ratio = 23.3/1, hydrothermal and), Cu ⁺ /Y-zeolite, Cu ⁺ /SiO ₂ (tetraethyl orthosilicate and Cu(NO ₃) ₂ ·3H ₂ O, sol-gel method)	2 °C, high pressure Hg lamp (λ > 280 nm), batch reactor, lower pressure (NO < 2 Torr) and higher pressure (NO ≈ 20 Torr)	N ₂ , O ₂ , N ₂ O	N ₂ , O ₂ and also N ₂ O (for higher NO pressure)	Cu ⁺ /ZSM-5 the highest reactivity	[135]
Low-loading (0.035–2.45%) TiO ₂ on the surface of ZSM-5 zeolite (Ti/ZSM-5, from HZSM-5 Nissan Girdler Catalysts and Ti(OC ₃ H ₇) ₄ Nacalai Tesqu, impregnation method)	500 W high pressure Hg lamp through a glass filter (Hoya U360), 10 Torr NO		N ₂ , O ₂ , N ₂ O		[136]
REVIEW (Pt or Rh)/TiO ₂ highly dispersed TiO ₂ species prepared within zeolite frameworks or silica matrices, TiO ₂ -based binary catalysts combined with Al ₂ O ₃ or SiO ₂ (sol-gel method or precipitation method), metal (mainly Cr-, V-) ion-implantation TiO ₂ catalyst, V-ion-implanted Ti/HMS and Ti/MCM-41, 2 °C	UV, Visible light irradiation (λ > 450 nm) also outdoor solar light (for metal ion implanted catal.)		TiO ₂ -zeolite: good selectivity for N ₂ and N ₂ in contrary to simple TiO ₂ (N ₂ O production)		[120]
Ti-oxide/Y-zeolite catalyst (Ti/Y: 1.1 wt% as TiO ₂ ; method: ion-exchange of the Y-zeolite (SiO ₂ /Al ₂ O ₃ = 5.5), aqueous titanium ammonium oxalate solution), Ti-oxide/Y-zeolite catalyst (method: impregnation, "Ti/Y-A": 1.1 wt%, "Ti/Y-B": 10.0 wt% as TiO ₂ , aqueous titanium ammonium oxalate solution), Ti-silicalite (TS-2, "TS-2A": 2.3 wt%, "TS-2B": 8.1 wt% as TiO ₂ , hydrothermal method), Ti-oxide/silicalite (Ti/SL: 8.0 wt% as TiO ₂ , impregnation method, aqueous solution of TiCl ₃), The powdered TiO ₂ catalysts (anatase 92%, rutile 8%) were supplied as a standard reference catalyst (JRC-TIO-4, the Catalysis Society of Japan), 150 mg	2 °C, 75 W high-pressure Hg lamp with a water filter batch reactor,		N ₂ , O ₂ , N ₂ O	The best N ₂ selectivity(91%) for ex. Ti/Y	[118]



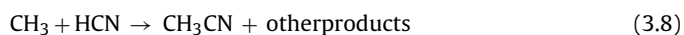
Eq. (3.3) is desired as the last step of NO photo-reduction in the presence of CO.

The mechanism of photo-SCR using CO as a reducing gas over other photocatalysts was described in the literature. Anpo et al. [69] proposed NO reduction in the presence of CO on a Mo-MCM-41 surface. They also concluded that the presence of this reducing agent strongly enhanced NO reduction. Roy et al. [55] presented another mechanism for NO photo-reduction on Pd ion-substituted nano-TiO₂ (Ti_{1-x}Pd_xO_{2-δ}, where x = 0.05–0.3). Bowering et al. [57] explained the function of silver loading on P-25 Degussa for the decomposition and reduction of NO in the presence of CO under UV light irradiation. Thampi et al. [61] proposed photo-NO reduction over TiO₂ modified by Ru, Rh and Cu. In general, loading of metals on the TiO₂ surface influenced the by-products (e.g., N₂O) formed and the N₂ selectivity.

The mechanism of photo-SCR of NO in the presence of hydrocarbons is still poorly understood. Stoichiometric mass balance reactions were proposed for the photo-SCR of NO in the presence of propane [60]:



Some researchers have not shown a detailed mechanism but have given information on by-products and possible reaction pathways. For example, Matsuoka et al. [59] explained that one of the products of NO reduction on a vanadium silicate-1 surface in the presence of propane under UV irradiation was CH₃CHO. In another photocatalyst system (Mo-MCM-41) presented by Anpo et al. [69], CH₃COCH₃ was created under UV irradiation. In this case, the following reaction mechanism was proposed: “the intermediate species formed between NO and the hydrocarbon radicals that are formed by H abstraction of the photo-excited Mo-oxide species from C₃H₇ subsequently reacts with NO to produce N₂ as well as oxygen-containing compounds”. It is also worth noting that propane was noticed to be a reactive reducing agent for photo-reduction of NO over different photocatalysts (e.g., Pd/TiO₂ [60], TiO₂ “Hombifine N” [54], VS-1, and Mo-MCM-41 [69]). Furthermore, Takeuchi et al. [70] investigated photo-reactions in a C₄H₈-NO₂-air system and concluded that one of the by-products of photo-reaction over ZnO under UV irradiation was HCN. Additional studies were subsequently reported by Takeuchi and Ibusuki [71], where many metal oxides (CeO₂, CoO, Cr₂O₃, Fe₂O₃, NiO, SnO₂, TiO₂, WO₃, ZnO, and ZrO₂) were tested as photocatalysts under UV irradiation. Acetaldehyde (CH₃CHO) was observed as one of the major products (besides CO and CO₂). In addition, cyano compounds (e.g., HCN and CH₃CN) were also observed. The generation of these compounds was explained by the interaction of NO or atomic nitrogen adsorbed on the photocatalyst surface. The cyanides were most likely produced via Eqs. (3.7) and (3.8). The researchers also observed that the less active photocatalysts (Cr₂O₃, CoO, NiO) led to greater HCN generation.



The above mechanism of NO+CO reaction was determined on the assumption of absence of water and oxygen. Thus, investigation of the impact of oxidizing compounds (e.g., H₂O and O₂) on photo-SCR is necessary. Water vapor, as one of the main products of fuel combustion, exists in most exhaust gases. It should be noted that there are still relatively few published studies on water-assisted photo-SCR; therefore, the particular mechanism of photo-SCR in the presence of water and oxygen requires further investigation. Section 5.2 briefly mentions that the presence of water or/and

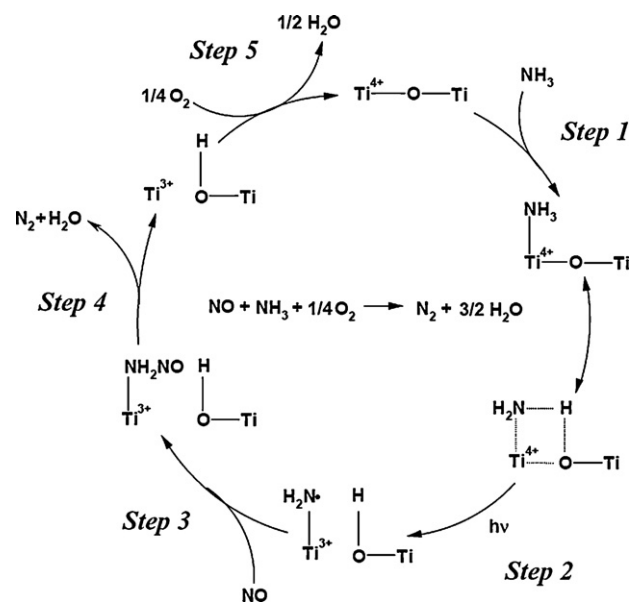


Fig. 2. Scheme of the mechanism of photo-SCR over NH₃ on TiO₂ surface [66] (needs permission; directly cited).

oxygen influences photo-SCR through the transformation of nitric oxide (NO) into NO₂, which is undesirable. We suggest that increasing temperature can inhibit this undesired reaction [54,63].

3.1.2. Reduction mechanism in the presence of NH₃

The overall reaction of photo-SCR with NH₃ is the same as that of thermal SCR (Eq. (2.1)). Teramura et al. [66] presented the mechanism of photo-SCR in the presence of NH₃ over TiO₂ photocatalyst shown in Fig. 2. They also determined the kinetic parameters and proposed the formula in Eq. 3.9, where *I* represents light intensity.

$$r = k C_{\text{NO}}^{\alpha} C_{\text{NH}_3}^{\beta} C_{\text{O}_2}^{\chi} I^{\delta} \quad (3.9)$$

They underscored that the intermediate product NH₂NO can be easily decomposed by heat treatment. An important supplement to this study would be the mechanism of NH₃ photo-oxidation in the presence of oxygen over anatase and rutile TiO₂.

3.1.3. Photocatalysts for photo-SCR in the presence CO or hydrocarbons

Improving photo-SCR is mainly performed by enhancing the photocatalyst activity. Usually, the activity of a simple photocatalyst is first determined and then the photocatalyst is modified. Bowering et al. [58] investigated the reduction of NO over Degussa P25 in the presence of carbon monoxide. Later, the same research group modified P25 with silver loading [57] and used CO as the reducing agent. The authors observed the first strong enhancement in N₂ selectivity (100%) for a TiO₂-based photocatalyst without using NH₃ as the reducing agent. Thampi et al. [61] modified the P-25 photocatalyst by loading Ru, Rh and Cu. Instead of photo-reaction under UV irradiation, they also investigated thermal SCR from 90 to 240 °C. Unfortunately, N₂O was observed as the major by-product. However, the presence of Rh and Cu increased the decomposition of N₂O. Additionally, Su and Wu [60] observed excellent NO photo-reduction efficiency over Pd/TiO₂ in the presence of propane under UV light irradiation. The efficiency dropped when Pd was transformed into PdO during the photo-process (especially when NO and O₂ were present). Thus, periodic regeneration of the photocatalyst (500 °C, 2 h at H₂ presence) periodically is needed for high efficiency. Furthermore, Roy et al. [55] observed very good activity for a modified Pd/TiO₂ (by impregnation) photocatalyst for

NO abatement in the presence of carbon monoxide. They also prepared Pd ion-substituted nano-TiO₂ (Ti_{1-x}Pd_xO_{2-δ}) and the highest activity was observed with 1% Pd. Finally, Matsuoka et al. [59] used a vanadium silicalite-1 photocatalyst (VS-1) to run a deNO reaction in the presence of propane under UV irradiation. Good activity was achieved by incorporation of VS-1 in a zeolite framework. The photocatalyst existed as isolated tetrahedrally coordinated V-O moieties on the zeolite surface. Therefore, enhancement of photo-deNO efficiency was achieved for V-containing and Mo-MCM-41 photocatalysts [72] in the presence of propane. However, the enhancement was not observed in the case of a Ti-MCM-41 photocatalyst.

3.1.4. Photocatalysts for photo-SCR in the presence of NH₃

A similar tendency, comparing to photo-SCR at C₇H₈ presence, was observed for photo-SCR in the presence of NH₃. The deNO_x efficiency was improved upon optimization of the photocatalysts. These optimization studies began using TiO₂ without additives. Teramura et al. [66,73] used commercial TiO₂ (P-25 and JRC-TIO-4) as photocatalysts and observed that the presence of oxygen in the gas mixture prevented N₂O formation during photo-reaction. Cant and Cole [68] used TiO₂ pressed wafers (85% anatase, 15% rutile) under UV light irradiation (photo-reaction at 30 °C) and at a higher temperature (300 °C) for thermal SCR. Yamazoe et al. [64,65] tested multiple metal oxides, including V, Cr, Mn, Fe, Co, Ni, Cu, Zn, Y, Zr, Nb, Mo, Ta and W, as supporting materials for TiO₂, but positive results were only obtained for Nb, Mo and W oxides. The best activity (92% NO conversion at GHSV = 16,000 h⁻¹) and the highest N₂ selectivity (99%) were achieved for 1% WO₃/TiO₂. The enhancement in photo-activity was explained by creation of isolated, tetrahedrally coordinated tungsten sites over the TiO₂. Furthermore, Jin et al. [67] prepared an Si-doped TiO₂ photocatalyst by the hydrothermal method and woven glass fabric was used as the supporting material. A 50% enhancement in photo-deNO activity was achieved compared to Degussa P25 under UV light irradiation with 3% O₂ at 50 °C.

3.2. Photo-oxidation

The aim of photo-oxidation is to transform NO into HNO₃ via the formation of HNO₂ and NO₂. The concept is the same as that for traditional NO_x absorption. The main advantage of this process is the higher possibility of NO conversion into NO₂ than into HNO₃ because the atmosphere contains considerable amounts of oxygen (e.g., exhaust gas ~5% vs. air ~21%). However, during photo-oxidation of NO, saturation of the photocatalyst surface by HNO₃ will occur, requiring consistent catalyst regeneration. Additionally, photo-oxidation may lead to HNO₃ creation, the storage or utilization of which can be troublesome.

Photo-oxidation of NO provides a way to remove NO_x emitted from stationary power plant sources or vehicle engines. Table 2 presents results cited in the literature. The table is divided into the columns photocatalyst (short explanation), conditions (light, composition of gas mixture, temperature), detected compounds, main products of reaction and obtained maximum efficiency. More specific information can be found in the literature (last column).

3.2.1. Oxidation mechanism

The NO photo-oxidation mechanism for TiO₂ photocatalysts undergoes three states (NO → HNO₂ → NO₂ → HNO₃) and is described by the reactions shown in Eqs. 3.10–3.18 [82,83,98,99]. Wang et al. and Dalton et al. proposed additional reactions for the mechanism, as shown in Eqs. (3.19)–(3.22) [90,99]

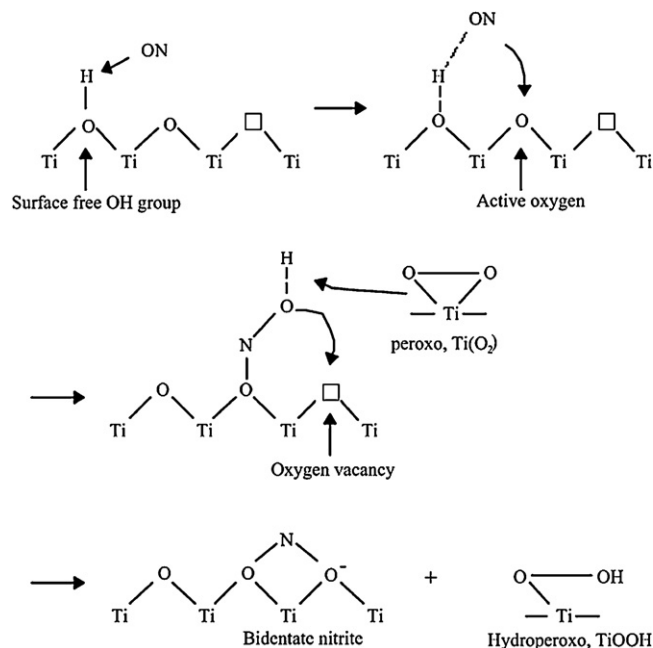
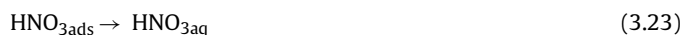


Fig. 3. A possible mechanism of NO adsorption on TiO₂ [112].



Eqs. (3.10)–(3.13) represent typical photocatalytic reactions including charge carrier generation (Eq. (3.10)) and the trapping of a hole and an electron to produce “active” hydroxyl and oxygen radicals (Eqs. (3.11)–(3.13)). The other equations represent oxidation reactions by hydroxyl radicals (Eqs. (3.14)–(3.17)) and oxygen radicals (Eq. (3.18)). Additionally, Dalton [90] suggested that deNO_x cycle must be closed by HNO₃ removal (water treatment) from the photocatalyst surface via the reaction in Eq. (3.23).



Wu and Cheng [112] carried out detailed analysis of photocatalytic reactions of NO on TiO₂ and transition metal-loaded M(Cu, V, and Cr)/TiO₂ using *in situ* FTIR spectroscopy. A possible mechanism for NO adsorption and oxidation on the TiO₂ surface is shown in Figs. 3 and 4. Initially, NO is adsorbed on the TiO₂ surface and then attacks free surface OH groups, which are oxidized by active surface oxygen, creating monodentate NOH species. These are subsequently transformed into bidentate nitrite and hydroperoxo (TiOOH) species. As shown in Fig. 4, electron–hole pairs are then photo-generated under UV irradiation and the peroxo (Ti(O₂)) is transformed into superoxo (TiOO•) by hole trapping. Because

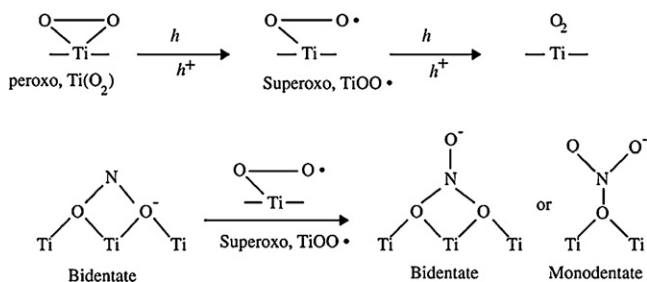
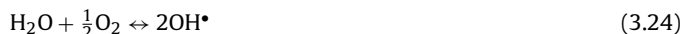


Fig. 4. A possible mechanism of NO oxidation on TiO₂ [112].

superoxo (TiOO•) is extremely reactive with very short lifetime, it oxidizes bidentate nitrite into monodentate or bidentate nitrate. If superoxo does not react with nitrites, it transforms into oxygen molecules. Wu and Cheng [112] emphasized the important role of the OH group and oxygen vacancies in photocatalytic reactions. They also proposed a mechanism of photo-NO oxidation on transition metal-loaded M(Cu, V, and Cr)/TiO₂. However, the most powerful activity was observed for pure TiO₂ [112].

Recently, Hunger et al. [78] and Ballari et al. [77] proposed kinetic models for photo-removal of NO_x under UV-A irradiation in concrete pavement containing TiO₂. The kinetic parameters were determined as a function of NO and NO₂ concentration, flow rate, humidity, and UV-A irradiance. The external mass transfer of the gaseous compounds and the internal molecular processes (diffusion, reaction) were also taken into account. The models were evaluated experimentally and model predictions showed good agreement with experimental results. Yu et al. [113] performed a kinetic study of photo-NO oxidation under visible light irradiation over commercial carbon-doped TiO₂ (Kronos, Germany). The model included the process parameters of volumetric flow rate of the pollutant, relative humidity, irradiance, pollutant concentration, reactor size and dose of the photocatalyst.

An important issue for effective photo-oxidation of NO is maintenance of process parameters (e.g., light intensity, light wavelength, residence time of NO_x in reaction zone, humidity and type of catalyst) at optimum levels. NO₂ (intermediate) can easily be released from the TiO₂ surface to the atmosphere if the process parameters are not maintained at a proper level. According to the literature, the relative humidity seems to be the most important factor, as a high concentration of hydroxyl radicals contributes to easier NO₂ transformation into HNO₃. The mechanism of photo-oxidation of NO to NO₃⁻ via NO₂ creation was recently confirmed by Folli et al. [114], who underscored the role of water in photo-oxidation on nano-sized TiO₂ (100% anatase). Hydroxyl radicals (OH•) play an important role in photo-reactions are created via the overall reaction:



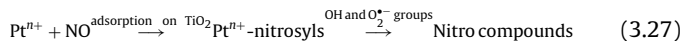
Hence, the photo-oxidation of NO depends strongly on the presence of water in the reaction. The strong dependency of photo-oxidation efficiency on relative humidity was also observed by Chin et al. [115].

Very recently Wu et al. [116] revealed the role of PtO and PtO₂ deposits in the photocatalytic oxidation of NO over a Pt-modified TiO₂ catalyst. A portion of PtO₂ on the surface of the Pt/TiO₂ was observed by *in situ* XPS to be reduced to PtO under UV irradiation. Thus, the PtO₂ was an electron trap. Photocatalytic activity was improved as a result. The photocatalytic reaction was tested in a continuous flow photoreactor under UV light irradiation ($\lambda = 300\text{--}400\text{ nm}$, 125 W Hg Philips lamp) with a gas mixture containing $\sim 100\text{ ppmv}$ NO in air (relative humidity $\sim 75\%$). PtO₂ particles dispersed on the TiO₂ surface were populated with the electrons generated during the photo-reaction. As a result, PtO₂

was transformed into PtO and O^{•-}, which could be oxidized into molecular oxygen via the reactions:



Palladium sites contributed to the adsorption of NO. According to the authors' explanation, formation of Pt⁰-NO nitrosyls and Ptⁿ⁺-NO mononitrosyls was possible. The irradiation of this system in the presence of OH• and O₂^{•-} led to the preferential oxidation of nitrosyls to nitro compounds. Based on this explanation, the mechanism of NO photo-oxidation on Pt/TiO₂ was proposed as follows:



3.2.2. Photocatalysts

Many investigators have tried to improve photo-NO_x oxidation by increasing the efficiency of the deNO_x process. The main aim of the photo-oxidation of NO_x is to apply the technique to real systems (e.g., industrial or other commercial systems). Efforts have focused on improving the photocatalyst, the experimental conditions (e.g., type of light, light intensity, gas mixture composition, and residence time) and the type of reactor. Many researchers used commercial TiO₂ (e.g., Degussa P25) as a reference photocatalyst against improved photocatalysts. For example, Ao and Lee [95] and Ao et al. [94] used commercial Degussa P25 and TiO₂ immobilized on an activated carbon filter. They elucidated the influence of humidity, residence time and VOCs on the efficiency of the photo-deNO_x process. They then focused on the simultaneous removal of NO_x and VOCs (benzene, toluene, ethylbenzene and *o*-xylene) at various humidities. Toma et al. [96,97,100–103] tried different plasma and thermal spraying processes for increasing the removal efficiency of NO_x. The highest deNO_x efficiency was 52% (calculated for NO) using a photocatalyst prepared as a fine particle coating. Plasma techniques (e.g., atmospheric plasma spraying (APS) or suspension plasma spraying (SPS)) and high-velocity oxygen fuel spray (HVOF) were also used [103]. Furthermore, TiO₂ was mixed with Al to create a TiO₂-Al composite coating, which was expected to improve the charge separation and enhance the photocatalytic activity [100].

Significant improvement of pollutant removal was observed for a TiO₂/C photocatalyst. Hashimoto et al. [117] investigated the influence of calcination temperature, crystal size and specific surface area on photo-NO oxidation efficiency of TiO₂. Decreasing calcination temperature or crystal size and increasing specific surface area improved activity. This result was reasonable because higher calcination temperatures lead to increased crystal size. The researchers also determined the qualitative and quantitative dependence of this phenomenon. In addition, superior activity was obtained when TiO₂ was loaded with palladium [81–83]. Wu et al. and Sheng et al. improved not only the NO conversion (72% higher than P25) but also decreased deactivation of the photocatalyst in comparison to commercial TiO₂. The investigators explained this result with charge trapping on the Pd surface. The proposed mechanism for NO oxidation on TiO₂/Pd is shown in Fig. 5.

Hashimoto et al. [104] mixed (mechanically) HyCOM (hydrothermal crystallization in organic media) TiO₂ with Y- and A-type zeolites. They concluded that for a mixing ratio of A zeolite:TiO₂=3.7, the activity of NO_x photo-oxidation was enhanced 3 fold in comparison to bare TiO₂. In addition, Ballari et al. [77] tested commercial concrete paving stones containing TiO₂. The experiments were carried out using a laminar flow photoreactor under UV-A (345 nm) irradiation. They then proposed a kinetic model for photo-NO_x oxidation and determined the kinetic coefficients for these chemical reactions.

The big challenge for researchers is improving the visible-light response of photocatalysts used for NO_x removal. Yin et al.

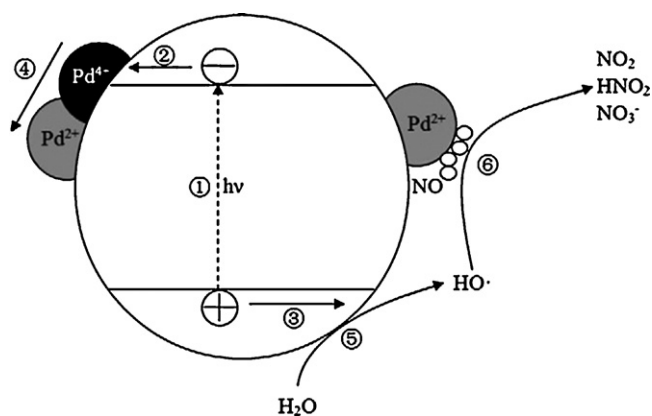


Fig. 5. Proposed mechanism of photocatalytic oxidation of NO over Pd²⁺ modified TiO₂. (1) band gap excitation (e⁻, h⁺) under UV illumination, (2) trapping of e⁻ by Pd⁴⁺ ions, (3) trapping of h⁺ at photocatalytic surface, (4) reduction of Pd⁴⁺ to Pd²⁺, (5) oxidation of H₂O to OH[·], (6) oxidation of NO to NO₂, HNO₂ and NO₃⁻ [83] (needs permission; directly cited).

[75,85,86] attempted to obtain visible responses for photocatalysts by doping TiO₂ with nitrogen and iron and platinum. The reactions [85] were carried out under visible light irradiation using an LED light source (red 627 nm, green 530 nm, blue 445 nm) or a high-pressure mercury lamp with filters (cutting <400 nm, <510 nm). They also used UV light (LED 390 nm and Hg lamp with filter to 290 nm) to run the experiments and compared the results with those obtained using visible light. The best results under the light spectra were obtained for nitrogen- and platinum-doped TiO₂. The efficiencies were 16, 28, 37, and 38% for red, green, blue and UV light, respectively. The authors also tried different techniques to obtain highly active N-doped photocatalysts (TiO_{2-x}N_y). They applied a homogeneous precipitation – solvothermal process in TiCl₃ – hexamethylenetetramine (C₆H₁₂N₄) aqueous and alcohol solutions [75] or mechanochemical doping [86]. For mechanochemical doping (high-energy ball milling of P25 titania), the best result was obtained when hexamethylenetetramine was used as the N precursor. They also tested urea and ammonium carbonate as N precursors. Fig. 6 shows the relationship between N-amount and activity of the photocatalyst using different nitrogen precursors. The photo-activity of TiO_{2(x)}N_y was dependent not only on the applied technique but also the amount of nitrogen in the photocatalyst.

Huang et al. [87] synthesized visible-light responsive PtO_x-doped TiO₂ (PtO_x-TiO₂) and PtO_x-loaded TiO₂ (PtO_x/TiO₂) photocatalysts and applied them to deNO_x oxidation under UV-, blue-, green-, and red-LED at 1 mW/cm². The authors emphasized that Pt oxidation state (reduced Pt⁰ or oxidized PtO_x) was important in the photo-deNO_x process. The highest visible-light activity was achieved for Pt/TiO₂ prepared by the sol-gel process and impregnated with H₂Pt(OH)₆ as the PtO_x dopant. The NO_x removal efficiency was ~55, ~52, ~49 and ~33% for UV, blue, green, and red light, respectively.

Hashimoto et al. [89] modified TiO₂ by loading platinum or rhodium chlorides to obtain H₂PtCl₆/TiO₂ (metal loading of 51 μmol/g) and RhCl₃/TiO₂ (metal loading 97 μmol/g) photocatalyst. They concluded that the oxidation rate of NO₂ to NO₃⁻ over RhCl₃/TiO₂ was faster than that over H₂PtCl₆/TiO₂. This was important because volatile NO₂ is more toxic than the non-volatile NO₃⁻. This photo-oxidation was carried out under visible (blue fluorescent lamp maximum energy at 450 nm, UV filter) and UV (black light, maximum UV energy at 369 nm) light irradiation. In addition, Tseng [88] synthesized visible-light responsive photocatalysts (sol-gel process using tetrabutylorthotitanate and

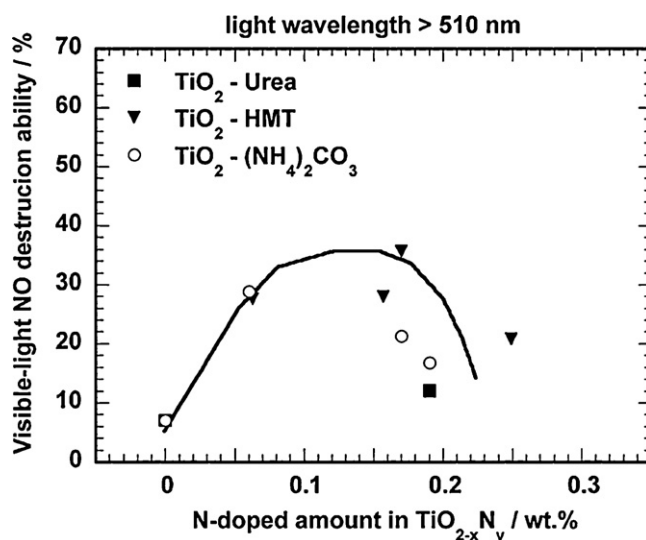


Fig. 6. Relationship between the nitrogen content and the visible-light photocatalytic activity for the wavelength of >510 nm. The samples were prepared by mechanochemical reactions of titania with (■) urea, (▼) HMT, and (○), (NH₄)₂CO₃ [86] (needs permission or re-change; directly cited).

ethanol under acid catalyzed conditions with controlled calcinations) based on TiO₂. The visible-light activity was expected to result from the impurities (carbonaceous species) as well as the mixing of crystal lattice anatase, brookite and rutile phases. The authors carried out the experiments under visible (LED: blue 465 nm, green 515 nm, and red 640 nm) and UV (lamp, 365 nm) light irradiation (1 mW/cm²). The best results (NO_x removal efficiency up to 70%) were obtained for a calcination temperature of 200 °C.

Yu and Brouwers [105] used commercial carbon-doped TiO₂ (Kronos, Germany) for photo-oxidation of NO under visible-light irradiation (day light lamps, λ = 400–600 nm). The photocatalyst was anchored on glass fibers and the whole fibers were sprayed onto a wool fabric. The maximum efficiency under visible-light irradiation was approximately 20% (57% for UVA irradiation). Additionally, Spadavecchia et al. [106] used N-doped TiO₂ nanoparticles in a batch reactor for photo-reaction under artificial solar irradiation (λ = 380–600 nm). The photo-conversion of NO_x was ~90% in 80–90 min under these conditions.

Recently, Chin et al. [115] obtained ultrafine nanopowder (10.5 nm) TiO₂ with large surface area. The material was characterized by a pure anatase phase and dense polyhedral structures despite the low degree of crystallinity. The researchers observed 10% improvement in deNO_x compared to commercial Degussa P25.

3.2.3. Processes

Researchers have tried different experimental conditions for improving photo-deNO_x processes, including modification of the photoreactors. Traditional continuous flow or batch reactors are typically used. However, modifications to the photoreactor are occasionally introduced to improve the photo-process rate or for modeling quasi-real conditions. For example, Matsuda et al. [84] employed a two-dimensional fluidized bed reactor (2 mm × 70 mm cross-section) with visual observation using a CCD video camera. They noticed that ultrafine TiO₂ particles (7 nm) provided better photo-activity than larger ones (20 and 200 nm). The apparent fluidization velocity was 23 cm/s and NO_x removal was carried out under UV irradiation in this study. In addition, Komazaki et al. [91] used an annular diffusion scrubber coated with TiO₂ in the scheme displayed in Fig. 7.

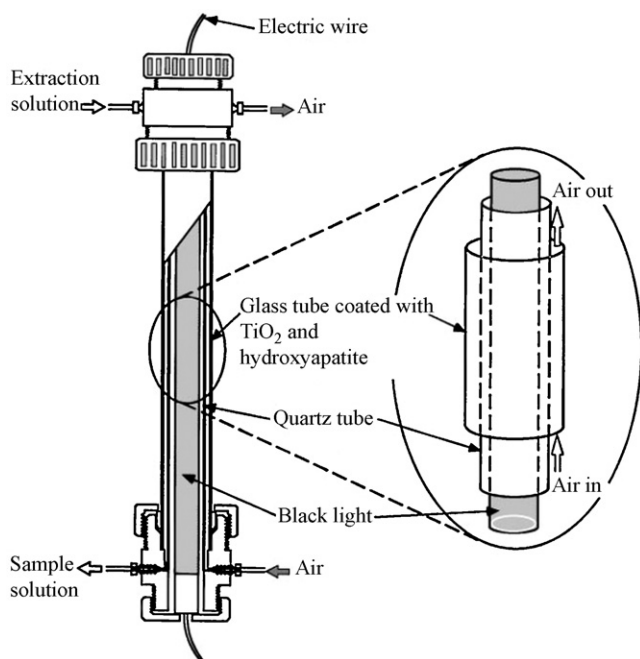


Fig. 7. Scheme of annular diffusion scrubber used by Komazaki et al. [91]. Specification of the reactor and experimental conditions: Outer tube: Pyrex-glass tube coated with TiO₂ and hydroxyapatite (21 mm i.d., 25 mm o.d.); Inner tube: Quartz tube (16.5 mm i.d., 19.5 mm o.d.); UV Black light (FL8BL, 8 W, NEC, Japan), Effective length: 25 cm; Air flow rate: 0.2–5.0 l/min (needs permission; directly cited).

Toma et al. [94,96,97,100–103] designed an experimental setup where the NO_x mixture was prepared *in situ* by chemical reaction between copper powder and nitric acid. The researchers also created a neural computational model to predict experimental results. The input data were the photocatalyst powder mass, the exposure time and the exposed surface area. The output results were NO and NO_x removal efficiencies [97]. Wu and Cheng [112] used a special reactor for *in situ* FTIR investigation of the reactions occurring on the photocatalyst surface in photo-NO oxidation. The concentrations of nitrogen compounds on TiO₂ and transition metal-loaded M(Cu, V, and Cr)/TiO₂ were measured under dynamic conditions. This system can also be utilized for investigating photo-processes at high temperature. The scheme of this reactor setup is shown in Fig. 8.

3.3. Photo-decomposition

The assumption for photo-decomposition of NO_x is that the process occurs via reaction on the photocatalyst surface (Eq. (3.28)). The development of a photocatalyst for NO_x photo-decomposition is focused on increasing the activity and selectivity towards N₂ production. Table 3 details selected studies on the photo-decomposition of NO_x. Most of the results have been done by Anpo's research group. More information about their investigations can be found in literature [69,118–120] and reference therein.



3.3.1. Decomposition mechanism

Possible mechanisms for NO decomposition on TiO₂ (Degussa P25) are listed in Eqs. (3.25)–(3.32) [58]. The dominant reaction is Eq. (3.31), where N₂O is generated as the major product.

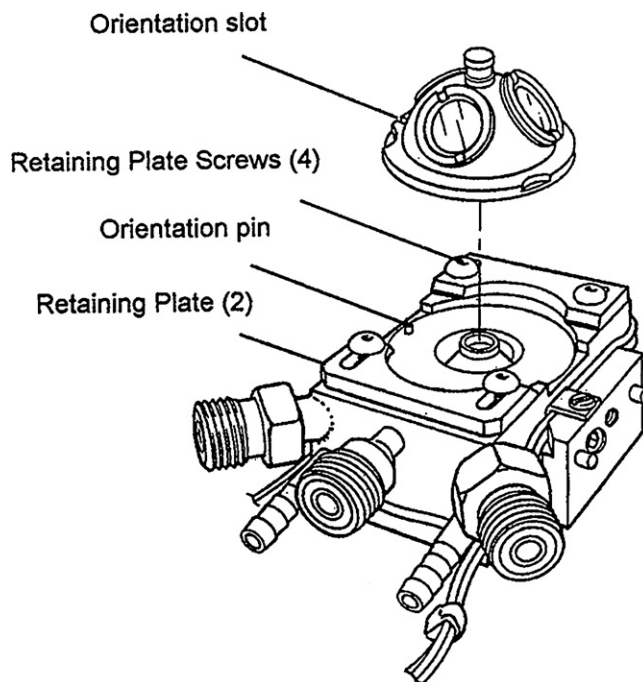
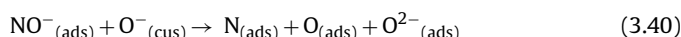


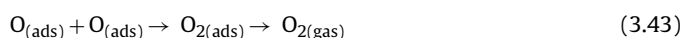
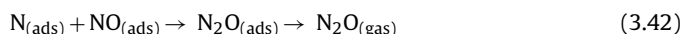
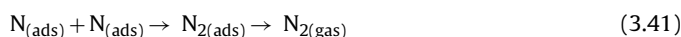
Fig. 8. Scheme of photoreactor used for *in situ* FTIR investigations by Wu and Cheng [112,187] (needs permission, directly cited).



Courbon and Pichat [48] and Cant and Cole [68] proposed similar mechanisms for NO photo-decomposition on TiO₂:



where the abbreviation “cus” is “coordinatively unsaturated oxide ions”. Gaseous compounds, such as N₂, O₂, and N₂O, are formed via the following reactions:



The nitrates are formed via the following reaction:



The rate of the reaction in Eq. (3.44) increases in the presence of high concentrations of gaseous oxidant compounds (O₂, H₂O). This phenomenon plays a more important role in photo-decomposition processes than photo-oxidation processes (see Section 3.2).

NO can also be transformed into N₂O or NO₂ depending on the reaction conditions (e.g., pressure, photocatalyst, light wavelength and intensity). Anpo and Takeuchi et al. [69,120] observed strong dependence for the coordination number of the Ti-oxide species and N₂ formation selectivity. TiO₂ can exist as highly dispersed and isolated tetrahedral species (e.g., Ti-oxide/Y-zeolite

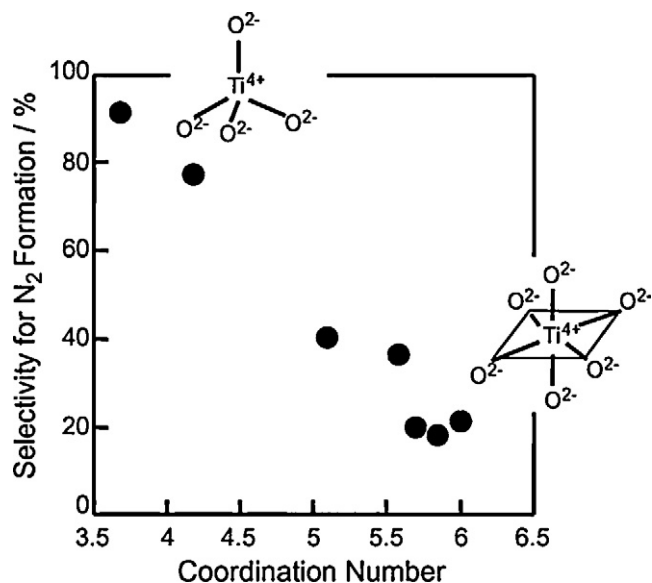


Fig. 9. Relationship between the coordination number of Ti-oxide species and the selectivity for N₂ formation in the photocatalytic decomposition of NO on various titanium oxide photocatalysts [69] (needs permission; directly cited).

photocatalysts prepared by ion exchange techniques) or as aggregated octahedrally coordinated Ti-oxide species (Ti-oxide/Y-zeolite photocatalysts prepared by impregnation). High efficiency and selectivity are obtained for Ti-oxide species with lower coordination number. The relationship between coordination number and selectivity for N₂ formation in NO decomposition is shown in Fig. 9. Additionally, titanium oxide species are excited by UV irradiation during photocatalytic reactions (Eq. (3.45)) to form excited complexes (Ti³⁺-O⁻)^{*}:



A tetrahedrally coordinated Ti oxide was confirmed by X-ray absorption near edge structure (XANES) and extended X-ray absorption fine structure (EXAFS) analysis technique. The behavior of the tetrahedrally coordinated Ti-oxide could be explained by the mechanism of NO reduction. The NO species is adsorbed onto the Ti-oxide as weak ligands to form the reactive precursors. Under UV irradiation, charge transfer excited complexes of the oxides, (Ti³⁺-O⁻)^{*}, are formed. Within their lifetimes, electron transfer from the trapped electron center, Ti³⁺, into the π-antibonding orbital of NO takes place and electron transfer from the π-bonding orbital of another NO into the trapped hole center, O⁻, occur simultaneously. These electron transfers lead to direct decomposition of two molecules of NO on (Ti³⁺-O⁻)^{*} into N₂ and O₂ even at 275 K. Such a mechanism provides high selectivity for N₂ formation and inhibits formation of undesired N₂O and NO₂ [69].

The lifetime of created holes and electrons on the isolated tetrahedral Ti-oxide species are longer than that on the aggregated octahedrally coordinated Ti-oxide species (aggregated or bulk TiO₂ photocatalysts). Thus, the conversion of NO into N₂ is preferable on the isolated tetrahedral Ti-oxide species. In this case, the formation of N₂O and NO₂ can be prevented.

3.3.2. Photocatalysts

The development of new or improved photocatalysts for photo-deNO_x is a big challenge for scientists and material engineers. Commercial TiO₂ (Degussa or others) is often used as a reference material. Improvements are evaluated by checking photo-activity with simple, powdered photocatalysts. Detailed information about

preparation and activity of different photocatalysts can be found in the literature [69,119,120,122,128].

Optimum properties were first investigated for powdered TiO₂ [47,48]. Courbon and Pichat [48] obtained approximately 50% selectivity for N₂ formation on TiO₂ powder (Degussa) under UV irradiation. The rest of the photo-decomposition product was N₂O. One of the major contributions to the development of photocatalysis was made by Anpo et al., who have improved many types of photocatalysts using the following objectives [69]:

- obtaining a more active tetrahedral structure (Ti- or Mo- or V- or Cr-oxide)
- increasing the selectivity for N₂ and the lifetime of the active structure
- increasing the deNO_x efficiency, and
- obtaining a photocatalyst that is active under visible light irradiation.

Yamashita et al. [118] and Anpo et al. [69] reported that in the case of powdered TiO₂, the selectivity for N₂ was only 25% (75% for N₂O). Anpo et al. [69] improved the photocatalyst activity by increasing the dispersion of Ti-oxide species and anchoring the photocatalyst onto silica glass or zeolite support. The ion exchange or impregnation methods were applied to obtain highly active photocatalysts. They noticed a high correlation between preparation method and Ti content for NO_x decomposition activity and N₂ selectivity. The best result (91% selectivity for N₂ with the highest activity) was obtained for a photocatalyst with 1.1 wt.% TiO₂ prepared by ion exchange. Titanium oxide was anchored on Al₂O₃ or SiO₂ to give a binary photocatalyst. Anpo and Takeuchi [120] observed increased selectivity for N₂ when the Ti content in the binary photocatalyst was decreased. They also emphasized the role of tetrahedral Ti-oxide for improving the efficiency of NO decomposition.

Anpo's group has tried different preparation methods (e.g., impregnation, ion exchange, and advanced metal ion implantation) and different supporting materials (e.g., silica glass, zeolites such as Ti-HMS, and Ti-MCM-41) for obtaining visible light responsive photocatalysts with high selectivity for N₂ [69]. Moreover, they also adopted the advanced metal ion implantation technique for obtaining visible light response photocatalysts. Anpo and Takeuchi [120] prepared V ion implanted Ti-HMS and Ti-MCM-41 photocatalysts and applied them to the decomposition of NO into N₂ and O₂ under visible light irradiation (λ > 420 nm). This technique can also be applied to bulk TiO₂ photocatalysts. The un-implanted or un-doped photocatalyst was not active under visible light irradiation. However, this technique requires the use of high accelerating energy to allow ions to be implanted into the oxide structure and obtain the desired effects. The catalyst prepared with lower energy will not generate the visible light active structure. The scheme for this advanced metal ion implantation method is shown in Fig. 10.

Anpo's research group also tried other photocatalysts based on a zeolite structure. For a Cr-HMS photocatalyst, the photo-activity under visible light irradiation was worse than under UV irradiation. However, the selectivity for N₂ was very high (97%) under visible light and only 45% under UV light. For V oxide species constructed within the framework of a zeolite structure (V/SiO₂ photocatalyst) and the Mo-MCM-41 photocatalyst, significant enhancement in NO reduction was observed in the presence of hydrocarbons (C₃H₈, CH₄, and C₂H₆) or carbon monoxide. Therefore, these photocatalysts can alternatively be applied to photo-SCR (see Section 3.1). Other studies performed by Anpo's research group used Cu⁺/ZSM-5 zeolite photocatalysts at 275 K [123,135], vanadium silicate (VS-2) [134], Ag⁺/ZSM-5 zeolite [123], highly dispersed titanium oxide

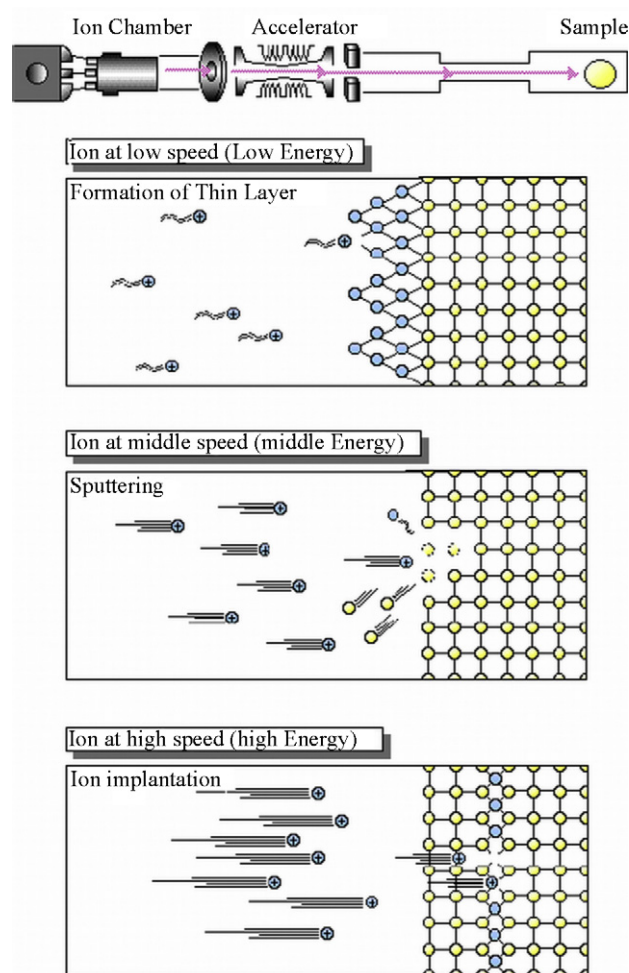


Fig. 10. Schematic diagram of an advanced metal ion implantation method [132] (needs permission; directly cited).

species [120], and transition metal oxides (e.g., Ti, V, Mo, and Cr) incorporated within the framework of zeolites [69].

3.3.3. Processes

Other ways of improving the deNO_x process include finding the best experimental conditions and proper reactors. This process is predominantly carried out in batch reactors [118,121,122,127,128,131,133–135] and sometimes in flow reactors [80,125,129,133]. Lim et al. [125] used two types of annular flow photoreactors, two serially connected reactors with the photocatalyst coated on a quartz reactor tube and a two-dimensional fluidized bed reactor. They investigated the influence of process conditions on NO_x decomposition over TiO₂ particles (Degussa P25) under UV irradiation. The authors investigated initial NO concentration, light intensity, process temperature, TiO₂/silica ratio and superficial gas velocity. The scheme of the fluidized bed reactor employed is shown in Fig. 11.

3.4. Section summary

Photocatalysis can be a very efficient method for NO_x abatement. In this section, we presented three methods of NO_x removal by photocatalytic reaction: photo-SCR, photo-oxidation and photo-decomposition. The most promising method seems to be photo-SCR, but it is also the most difficult process to employ for real applications. All the described photo-deNO_x processes have their advantages and weaknesses (Table 4). Nevertheless, it is believed

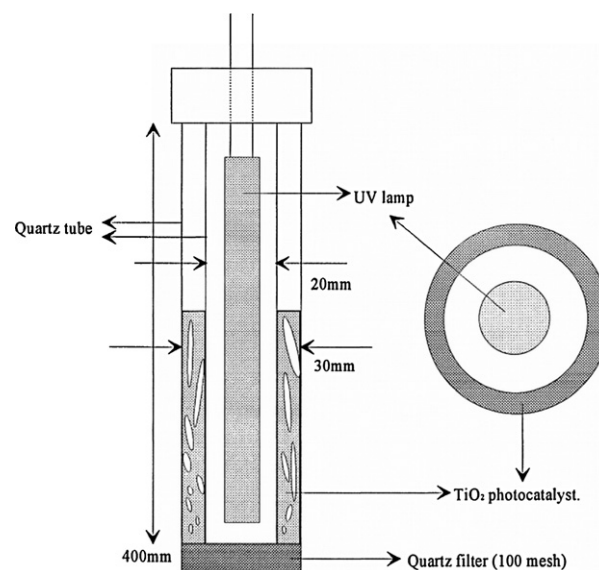


Fig. 11. Two-dimensional fluidized bed reactor used by Lim et al. [125]. *Experimental conditions:* 0.12 g TiO₂/silica (Degussa P25, silica gel 202–355 μm, Merck, ratio: 0.07–0.33), flow rate 88–826 ml/min, 106 ppmv NO/He, four fluorescent black light lamps (8 W, Sankyo Denki, Japan, F8T8 max intensity at 365 nm) and four germicidal white light lamps (8 W, Sankyo Denki, Japan, G8T8, max intensity at 254 nm) (needs permission; directly cited).

that the limitations can be eliminated through continuous scientific investigation.

4. Applications

In Section 3, we showed the results from investigation of photo-deNO_x processes. The research was carried out on laboratory scale for better understanding of the NO_x reduction mechanism under UV and visible light. Furthermore, the researchers tried to improve photocatalyst activity and optimize experimental conditions for NO_x removal efficiency. The final goal of developing photo-deNO_x processes is to apply them to commercial systems. It is worth noting that research on photo-deNO_x was carried out on a large scale (204 m³) at the European photoreactor (EUPHORE) in Valencia, Spain (Fig. 12). The EUPHORE is equipped with several useful analytical instruments including an *in situ* FTIR spectrometer, a GC, an HPLC, a GC–MS, analyzers for numerous gases (e.g., NO/NO_x/NO₂, ozone, CO, CO₂, total hydrocarbons (THC), O₂), light intensity radiometers and a modern diesel engine (Lynx V277 90 PS Ford Focus engine) for the supply of exhaust. The synergetic reactions of NO_x, HC, ozone and other gaseous compounds were investigated under solar-light irradiation [137–140].

Table 4

Advantages and limitations of photocatalytic processes for NO_x removal.

Advantages	Limitations
Use of renewable and accessible source of energy	Catalyst sensitivity and possibility of catalyst damage (e.g., at SO ₂ presence)
Savings of energy and natural sources (fossil fuels)	Lower reaction rate in comparison to thermal catalysis
Prevention of CO ₂ emission	Usually, faster catalyst deactivation
Applied "green chemistry"	Rather UV light is preferable
Clean and prospective technology	
Possibility of co-existence with traditional deNO _x methods (primary and secondary)	

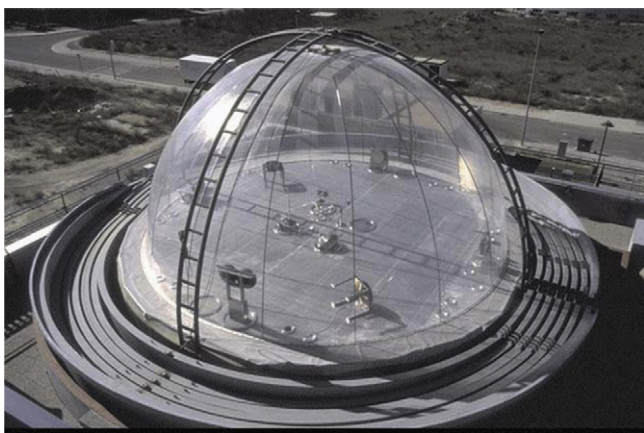


Fig. 12. The European Photoreactor in Valencia, Spain [139,140] (needs permission; directly cited).

In this section, the application of photocatalytic materials and the results are given for real cases. New photocatalytic materials or processes very often appear in patent applications because photocatalysis has been a very attractive field for commercial applications. It should be mentioned that NO_x can be produced from the atmosphere (environmental NO_x) and from flue gas generated from combustion (end-pipe NO_x).

4.1. Investigation of photocatalysts for real applications

Investigation of new photocatalysts eventually ends with real applications. For this purpose researchers attempt to create real or quasi-real conditions for testing new materials. Before utilization, a new material should be tested to see if it can be used in commercial applications. For example, Hunger et al. [78] used concrete paving blocks for NO_x removal in European cities. The main research aim was to determine the kinetic coefficient of the photo-de NO_x process. They concluded that the kinetic parameters could be used to model real applications using CFD methods. Maggos et al. [141] investigated two types of photo-active paints (containing 10% TiO_2): mineral silicate paint and styrene acrylic paint. The experiments were carried out in a real-scale environmental chamber (30 m³) under UV light irradiation. The initial concentration of NO was 220 ppb and the process was photo-oxidation of NO. The impact of relative humidity (RH) on de NO_x efficiency was also investigated. Increasing RH from 20% to 50% significantly inhibited NO_x removal. The maximum efficiency for the mineral silicate paint and the styrene acrylic paint were 74% NO, 27% NO_2 and 91% NO, 71% NO_2 , respectively.

Similar investigations [142] were carried out in a real-scale car garage (322 m² covered by white acrylic paint including 10% TiO_2). The real exhaust gas from a car engine was introduced into the garage. Photo-oxidation of NO_x was then carried out under UV irradiation. The researchers noticed that increasing CO concentrations increased NO_x removal, but the presence of VOCs inhibited this process. The maximum efficiency was 19% for NO in this system. In addition, Maggos et al. [143] tested building materials (containing 3% TiO_2) for NO_x removal in pilot-scale street canyons (three streets, width: 2 m; height: 5.2 m; length: 18.2 m). The exhaust gas containing nitrogen oxides was introduced into the canyon by a pipe distributor. The gaseous compound (NO_x , SO_2 , CO, CO_2 , and TVOCs) concentrations were then continuously measured. The experiments were carried out under solar irradiation (continuously monitored) and meteorological parameters, such as wind direction, wind speed, temperature, and relative humidity, were measured. The NO_x concentrations measured in the TiO_2 canyon



Fig. 13. The Dives in Misericordia Church, Rome, Italy. Outside surface of the church was coated by cement including TiO_2 [145] (needs permission; directly cited).

were 36.7–82.0% lower than the ones recorded from the reference canyon.

Chen et al. [144] designed and investigated photocatalytic coating elements on road pavements for NO_x removal. They tested a cement concrete slab containing a TiO_2 photocatalyst under artificial daylight irradiation (3 × 50 W daylight lamps, Philips, Model # F36T12/D/HO, irradiation density of 250 W/m², inlet NO concentration of 2500 ppb) and obtained more than 90% NO conversion (photo-oxidation). The authors also tested the impact of inlet NO concentration on NO_x removal efficiency, and high NO removal efficiency was obtained for residence times between 5 and 20 min.

4.2. Photo-de NO_x processes and materials applied in real applications

Photocatalysts for NO_x abatement are used not only in pilot-scale reactors but also in real commercial objects, particularly building materials. For example, Guerrini and Corazza [145] claimed that the first application of cement containing TiO_2 was in 1996 within the three large symbolic sails of the “Dives in Misericordia” Church (Rome, Italy; see Fig. 13).

Guo et al. [146] collected interesting examples of TiO_2 -based building materials for removal of poisonous compounds (including NO_x) from air. In this paper, many examples of photo-active materials were described (exterior: paints, tiles, glass, plastics, aluminum panels; interior: wall paper, paints, window blinds; and road construction: soundproof walls, tunnel walls). Taoda [147] claimed that photo-active materials not only have good properties for the removal of NO_x or other pollutants, but are also recognized as more practical and esthetic. Interesting examples of pedestrian sidewalks constructed with TiO_2 -containing permeable blocks were also included, as were TiO_2 -containing adsorbents as decorative elements (Fig. 14). As shown in Fig. 14(c), the decorative element can function well if it is situated in open-spaces where UV light (from sunlight) is available, such as balconies and terraces.

Anpo [133] gave the example of soundproof highway walls coated with TiO_2 photocatalysts for the abatement of NO_x constructed in Osaka in April 1999. Hamada et al. [148] showed de NO_x construction applied in airports including Tokyo International Airport (Haneda Airport) and Ishigaki Domestic Airport (Okinawa prefecture). TiO_2 was used as the photocatalyst in these cases and 10–30% NO_x reduction was obtained. Examples of materials and technologies based on TiO_2 photocatalysts for de NO_x processes (e.g., tiles, porous ceramics filters coating traffic tunnels, paved roads and buildings with TiO_2 , indoor air cleaners) are described in the reviews of Fujishima and Zhang [149] and Carp [150]. Furthermore, Venturini and Bacchi [151] gave examples (Rogoredo and Monza, Italy) of substances (including TiO_2) sprayed onto asphalt

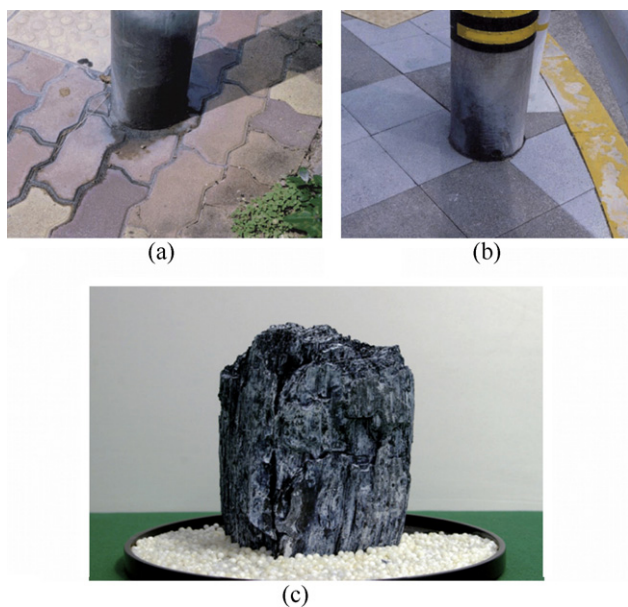


Fig. 14. Application of photo-materials including TiO_2 . Comparison of traditional permeable blocks, (a) with antifouling surface including photocatalyst (b) and photocatalytic functional adsorbent as decorative element c) [147] (needs permission; directly cited).

pavement surfaces for the removal of NO_x and other pollutants in air.

Recently, Laufs et al. [152] presented a study of photocatalytic oxidation realized using commercial TiO_2 -doped facade paints (white and blue). A commercial material (Kronos Int.: vlp 7000) containing a carbon-doped titanium dioxide in anatase modification (photo-activity under UV and visible (<500 nm) irradiation) was used as an active photocatalyst. The experiments were carried out in a flow photoreactor under simulated atmospheric conditions. The main products of photo-reaction were nitric acid and nitrate anion ($\text{HNO}_3/\text{NO}_3^-$). The model atmosphere (air containing 25–1000 ppbv NO_x ($\text{NO} + \text{NO}_2$), humidity ~50% r.h.) was introduced into the cylindrical flow tube photoreactor (1400 ml, 5.5 cm ID) and the irradiation conditions were maintained similar to atmospheric conditions ($\sim 57 \text{ W/m}^2$ for $\lambda < 380 \text{ nm}$). The authors then proposed application of photocatalytic paint in a street canyon. According to the model calculations, average photocatalytic reduction of nitrogen oxides in a typical street canyon (20 m width, $S/V = 0.1 \text{ m}^{-1}$) was only 5%. They explained that such low efficiency was due to the low ratio of surface to volume ($S/V = 0.1$ is typical for a street canyon). They mentioned other investigations that showed 40–80% removal efficiency, but the S/V in these cases was one order of magnitude higher.

Chen and Chu [153] recently showed results for photo-oxidation of NO_x using photo-active concrete pavements containing TiO_2 (anatase, diameter of 10–30 nm, specific surface area of $50 \text{ m}^2 \text{ g}^{-1}$) and activated carbon (prepared from granular coconut shells, mechanically ground into particles of less than $80 \mu\text{m}$). The tests were carried out as indoor and outdoor simulation experiments. The indoor tests involved experiments using a stainless steel batch reactor. The maximal deNO and deNO_2 efficiencies were 78.2% and 58.5%, respectively. However, after regeneration of the active surfaces with water flushing, the deNO and deNO_2 efficiencies were maintained at 63.1% and 43%, respectively. The other experimental conditions were a light intensity of 0.3 mW/cm^2 , relative humidity of ~50%, and a residence time of 125 s.

The outdoor tests were carried out under real road conditions. Some parts of the road at the Zhonghe Toll Station on federal highway G11 from Tsitsihar to the Nehe River (China) were covered by

concrete containing TiO_2 . Measurements were recorded in summer and winter during the daytime from 06:00 to 18:00. The maximum deNO_x efficiency was 24.1% during the summer time. Some factors should be taken into account in determining the deNO_x efficiency under outdoor conditions. First of all, it is not so easy to determine a contact time or GHSV in these cases. These parameters depend on wind (direction, intensity), which is turbulent or diffusion-controlled mixing of air. Moreover, TiO_2 (anatase) was applied as a photocatalyst and was active under UV light irradiation. Natural sunlight contains only 3–5% UV light, thus full utilization of sunlight is limited. Chen and Chu concluded that the photo-degradation of NO_x was related to light intensity and temperature, and 24.1% NO_x removal efficiency was quite good.

4.3. Patents

Rapid development of commercial photo- deNO_x technology is confirmed by the many patent applications submitted in the US, Europe or other countries. In this section, patents, not scientific research, are briefly reviewed. This section is divided into two parts: “Materials” and “Installations and applications”. In the first part, examples of photocatalysts or materials for photo- deNO_x processes are presented. In the second part, the application of photo- deNO_x processes, such as purifying installations, and the application of photocatalysts for soundproofing walls and real objects are presented. The processes are further divided into two groups, “end-pipe deNO_x processes” and “environmental deNO_x processes”. This concept, in a certain sense was adopted from Paz’s work [154] that overviewed patents dealing with TiO_2 .

4.3.1. Materials

Among the examples explored in this section, the main goal was obtaining materials with better photo-properties for NO_x abatement and that are multi-functional and easy to use. For example, Hayakawa et al. [155] revealed functional photo-materials (as $0.1\text{--}5 \mu\text{m}$ layers) based on TiO_2 mixed with copper or silver. The authors proposed a preparation procedure at low temperature ($\sim 300^\circ\text{C}$ or lower) and recommended the use of this material as antimicrobial agents and for deodorizing or decomposition of harmful substances. In addition, Tsujimichi et al. [156] reported composite material including TiO_2 as a photocatalyst and an amphoteric metal oxide or a basic metal oxide (e.g., barium oxide or strontium oxide). They recommended this photocatalyst for photo-oxidation of NO into nitric acid via NO_2 . The composite material could be further modified with other compounds such as Ag, Cu, Pd, Fe, Ni, Cr, Co, Pt, Au, Rh, and Ru for improved deNO_x efficiency. Ohmori et al. [157] created a composite photocatalyst (as a film) based on TiO_2 containing ZrO_2 (2:100 by weight). They recommended using the photocatalyst in photo- deNO_x processes under UV irradiation. It could also be used as a stain-resistant material (for buildings, exterior elevation, window frames etc.) or an antimicrobial agent.

Gambarelli and Pozzi [158] reported ceramics (tiles and trim pieces) with a special layer of TiO_2 (anatase, 1–25%). The thick layers also included microchannels that enhanced the permeability of water and increased the specific surface area. These ceramics showed higher activity for the removal of harmful substances and was recommended for photo-oxidation of NO_x .

Sugihara [159] disclosed visible light (400–600 nm) active photocatalysts for the photo-oxidation of NO_x . The photocatalyst was obtained by treating TiO_2 with hydrogen plasma or plasma of rare gases. Stable oxygen defects were observed in the TiO_2 structure (anatase or rutile phases) that were responsible for the enhanced photo-activity.

Aido [160] proposed a method for preparing panel-shaped ceramics that contained TiO₂ for effective removal of NO_x from the atmosphere. These ceramics could be used as sidewall construction material. In addition, Ji et al. [161] disclosed a photocatalyst for the removal of formaldehyde, toluene, VOCs and NO_x from air. The photocatalyst was a mixture of tourmalinite micro-particles (core) and titanium oxide nano-particles doped with Re metal and/or other transition metals. Han [162] presented a method for preparing eco-friendly paint that contained TiO₂ (3–10 wt.%) and could be used for purification purposes (e.g., antibacterial agent, sterilization, decomposition of organic contaminants, NO_x removal). Furthermore, Huder [163] presented a porous photocatalyst that was structured to allow penetration of light into the photocatalyst. The extremely large surface area significantly enhanced the photocatalytic activity of the reaction.

4.3.2. Installations and applications

The utilization of developed photo-materials in processes, installations or objects is obviously the next step after patent application. Researchers attempt to show new installations for NO_x removal using different methods, such as process parameters and co-application with another installation. These examples can be divided into two main groups: “end-pipe deNO_x” and “environmental deNO_x” processes. The end-pipe processes include the application of deNO_x concepts in a closed, determined system such as reaction chambers, reactors, and installations where process gases (e.g., exhaust gas) are cleaned. Environmental deNO_x processes describe the application of deNO_x processes for air cleaning (indoor and outdoor) using photo-active catalysts contained in decorative elements, soundproof walls and others.

4.3.2.1. End-pipe deNO_x processes. Taoda et al. [164,165] proposed a photo-installation for NO_x and other pollutant removal (e.g., VOCs). The installation was connected to the flue duct of a large-scale incineration furnace. The pellets coated with TiO₂ and loaded with different metals (e.g., platinum, rhodium, ruthenium, palladium, iron, silver, copper and zinc) were used for photo-reactions carried out at room temperature under UV light irradiation. Kagitani et al. [166] claimed an installation that included a photoreactor for the removal of NO_x emitted from automobile engines. The NO_x removal was carried out under UV irradiation (low voltage mercury lamp) for air-mixed exhaust gas with ammonia (NH₃:NO_x ratio ranged from 1.5 to 2:1). The photo-reaction of NO_x and NH₃, as well as the photo-oxidation of hydrocarbons and CO, was occurred. Particulate materials, such as oxide products, and ammonium present in the reactor were removed with a wet type electric dust collector. Wu [167] disclosed a combined wet absorption and photo-oxidation (under UV irradiation and in the presence of TiO₂) process for the removal of NO_x contained in smoke. The process exhibited high NO_x removal efficiency (60–90%), non-poisonous final products and low cost. This technology can be utilized for end-pipe NO_x abatement.

4.3.2.2. Environmental deNO_x processes. Kawai and Tatsumi [168] constructed a filter that contained a porous light emitting semiconductor (containing gadolinium). Titanium isopropoxide (Ti(OC₂H₅)₄) was dissolved in ethanol and sprayed onto the surface of the GaN whiskers of the sample, after which it was heated for 1 h at a temperature of 500 °C in air to coat the GaN surface with active TiO₂. UV irradiation was generated upon applying a voltage. The main function of the filter was to decompose organic matter, bacteria and viruses. However, the researchers noticed that the initial concentration of NO_x dropped from 100 ppm to zero during the first 2 h of operation of the filter. They attributed this phenomenon to photocatalytic NO_x removal. When voltage was applied, UV light with a wavelength of 365 nm was emitted. The filter could be used

for the decomposition and removal of other poisonous or undesirable substances, such as SO_x, CO, diesel particulates, pollen, dust, mites and other contaminants from air.

Hokkirogawa [169,170] disclosed an air-purifying, soundproofing wall that was recommended for photo-removal of NO_x emitted on highways. A single element of the wall was 50 cm × 50 cm × 2 cm and a 100 W black light lamp was used as the UV source. The wall included TiO₂ and its photocatalytic properties were tested in atmospheric air that contained 10 ppm of NO_x at a relative humidity of 70%. The 10 ppm NO_x was completely removed in 100 minutes. Additionally, Schwaag [171] disclosed a decorative screen for the removal of NO_x in air. The TiO₂ photocatalyst was coated or dispersed on the base material. The active surface of the photocatalyst was increased using different shapes (e.g., fins, ridges, dimples, holes) or by making it into different forms (e.g., foams, aggregates, webs, weaves or felts). The authors only emphasized comparison of the decoration quality and the de-pollution performance. However, the authors did not report the reaction conditions and the deNO_x rate.

Saito et al. [172] disclosed a soundproofing wall with good performance in NO_x and SO_x removal. The photo-active layer of the wall contained TiO₂ and pollutants such as NO_x and SO_x were transformed into HNO₃ and H₂SO₄ by reaction with water found in air or rainwater. Similar results were reported by Shigaya [173]. The photocatalyst was adhered on a honeycomb-shaped metal plate. The soundproofing wall was transparent because synthetic resin was used as the supporting material. Thus, the drivers and passengers were able to see the scenery outside. The NO_x and SO_x were transformed into HNO₃ and H₂SO₄ by photo-reaction in the presence of water.

5. Future trends and challenges in photo-deNO_x

Many photo-assisted processes are utilized in real applications. Photo-oxidation and photo-decomposition are the commonly applied methods in commercial processes. The most important goal in these applications is to search optimal conditions and photocatalysts for maximum NO_x removal. Additionally, results for photo-SCR under real conditions (e.g., exhaust gas) are difficult to obtain. The main problem is that water favors the transformation of NO into NO₂ and will decrease photocatalyst activity. Negative results can also be caused by the presence of SO₂, halogens and dust.

5.1. Proposed combination of photo-deNO_x with other primary or secondary methods

We believe that it is possible to combine primary methods (e.g., reburning and EGR), secondary methods (SCR) and photo-SCR into a high efficiency de-pollution system. Fig. 15 shows a simplified scheme for an industrial boiler system using photo-SCR. We consider three main zones where the photoreactor could be placed in the boiler system:

- at the flue gas recycle system (co-existence with an EGR system),
- at the traditional SCR system, and
- inside the convective chimney draught system.

The main advantage of this combined process is increased deNO_x efficiency through incorporation of traditional NO_x abatement methods with photo-processes. The reaction processes “A” and “B” in the proposition include photo-SCR in the presence of CO and hydrocarbons (Eqs. (3.1)–(3.6) in Section 3.1). The reducing agent could be commercial LPG gas or others. The most promising but more difficult to control location for the photoreactor is the

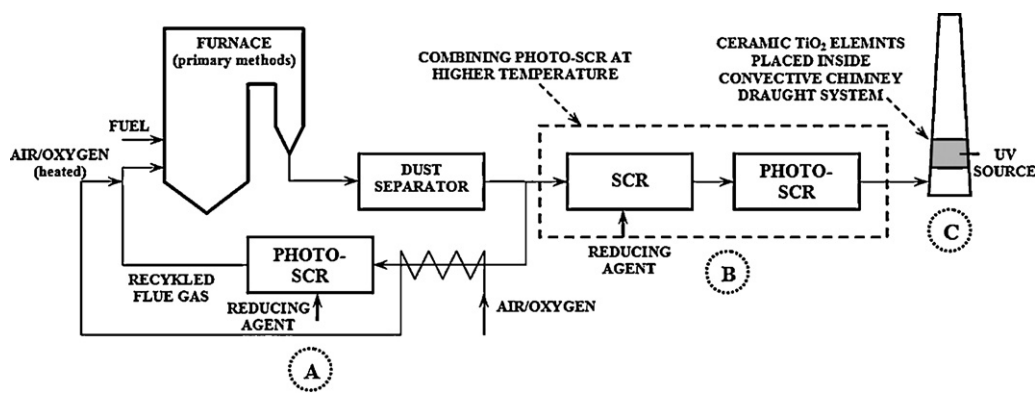


Fig. 15. The simplified scheme of photo-SCR applying in industrial boiler system: "A" with EGR system, "B" at traditional SCR system, "C" inside chimney draught system.

flue gas recycle system (zone "A" in Fig. 15). The process would adopt a primary deNO_x process and create a new technology that is attractive and advanced. Excess reducing agent could be introduced to obtain high NO_x removal efficiency [60]. The addition of excess hydrocarbons will increase the removal efficiency of NO_x, but the unreacted fuel will not be lost because it is burnt in the main furnace combustion zone. The gas mixture (original exhaust + reducing agent) will return back to the combustion zone. The temperature of the exhaust gas must be decreased because high temperatures (above 200 °C) are not desirable in photo-processes. This is why a heat exchanger should be placed before the photoreactor.

Decreased photo-activity with increasing temperature is not a general rule. It is often observed that an optimal temperature window for photo-processes exists. For example, Lasek et al. found that the optimal temperature window was 70–100 °C for photo-SCR of NO_x [63]. Further increasing the temperature decreased deNO_x efficiency. In addition, Brief description of the temperature window in different photo-processes can be found in their work. Chen and Chu concluded that as temperature increased, the reaction rate (in the photo-oxidation of NO_x over a concrete road surface containing TiO₂) decreased [153]. However, they explained that higher environment temperatures decrease the adsorption affinity of water rather than that of NO_x on activated concrete road surface, which results in the higher efficiencies for NO_x decontamination. In other words, as the temperature increased, the affinity of water decreased faster than NO_x.

Serial connection of a photoreactor with a traditional SCR (zone "B" in Fig. 15) is more practical and cost-effective. The two-reactor system can be combined to work at higher temperatures. The reaction process is the same as process "A", but the reducing agent is not used in excess. Therefore, the efficiency cannot be as high as "A", but the thermal SCR should be enough to remove most of the NO_x.

Photocatalysts can also be placed in the convective chimney draught system (see "C"), but photo-oxidation will occur in this arrangement. In this case, the internal chimney surface (covered by photo-active paint) should be regenerated periodically because the activity of the photocatalyst will decline. However, this arrangement seems to be the simplest and it can be applied more easily than "A" or "B". Usually, an exhaust gas monitoring system is placed on the platform surrounding the chimney and gas samples are taken directly from the chimney zone using a special slot. Thus, an active photo-surface and a light source can be placed under the monitoring slots.

5.2. The influence of water and oxygen in photo-SCR

As mentioned, an important problem for photo-SCR application is the presence of water and oxygen in real exhaust gases. The

surface of TiO₂ becomes superhydrophilic under UV light irradiation [174,175]. If water is adsorbed on the TiO₂ surface, it creates a very thin layer of water that inhibits photo-SCR. The transport of reactants and the products from the photocatalyst surface into the gas zone is also resisted by the formation of a water layer. Additionally, the presence of water, an oxidizer, will induce the formation of harmful NO₂. Hoffman et al. [176] thoroughly investigated the influence of OH groups on NO₂ formation in the presence of hydrocarbons. They used an excimer laser (248 nm) and an Ar⁺-laser as light sources. The OH radicals were thus produced from H₂O₂ photolysis. Muto and Takizawa [177] investigated homogenous photolysis of eight hydrocarbons (*n*-hexane, toluene, *n*-octane, *o*-xylene, *m*-xylene, propene, isobutene, and 2-methyl-2-butene; 30 ppmv or 10 ppmv) in the presence of NO, NO₂, O₂, H₂O and C₂H₅ONO under UV light (360 nm) irradiation. The creation of NO₂ is not desirable for photo-SCR because the final products should be non-poisonous.

Similar results can be observed for gases with high concentrations of oxygen. Poulston et al. [54] tried to resolve this problem by increasing the reaction temperature. They observed that under UV irradiation at higher temperature (150 °C), NO was transformed into N₂ or N₂O, even in the presence of significant amounts of oxygen (12%). They tested TiO₂ as the photocatalyst and several hydrocarbons (C₄H₁₀, C₃H₈, C₃H₆, C₂H₆, and C₂H₄) as reducing agents, concluding that NO was transformed into mostly NO₂ when the process temperature was below 42 °C. Moreover, Takeuchi and Ibusuki [71] tested photochemical reactions on gaseous mixtures of C₃H₆-NO₂-dry air under UV light irradiation over different metal oxides (CeO₂, CoO, Cr₂O₃, Fe₂O₃, NiO, SnO₂, TiO₂, WO₃, ZnO, and ZrO₂). It was noteworthy that they used fly ash samples obtained from the electrostatic precipitation of coal-fired power plants as the photocatalyst. Ibusuki and Takeuchi [178] further investigated toluene oxidation in the presence of O₂, NO₂ and H₂O under UV light irradiation over TiO₂. They observed that NO was one of the by-products and relative humidity strongly influenced the NO₂ and NO concentrations in the gas mixture. At 30% relative humidity, minimal NO was produced from the reaction between NO₂ and toluene.

Takagi et al. [179] considered the mechanism of *o*-xylene photo-oxidation (homogeneous) in the presence of NO and water. An optimal concentration of water was found for the photo-SCR system. However, the "water" problem should be considered if photo-SCR is applied in real industrial systems. The main issue is therefore determining the optimal conditions for photo-SCR of NO_x in the presence of water and oxygen. From a literature review, it can be concluded that important factors for improving deNO_x efficiency are temperature and the concentrations of water, oxygen and reducing agent.

We attempted to find the optimal conditions for photo-SCR under humid conditions using literature data. For example, a

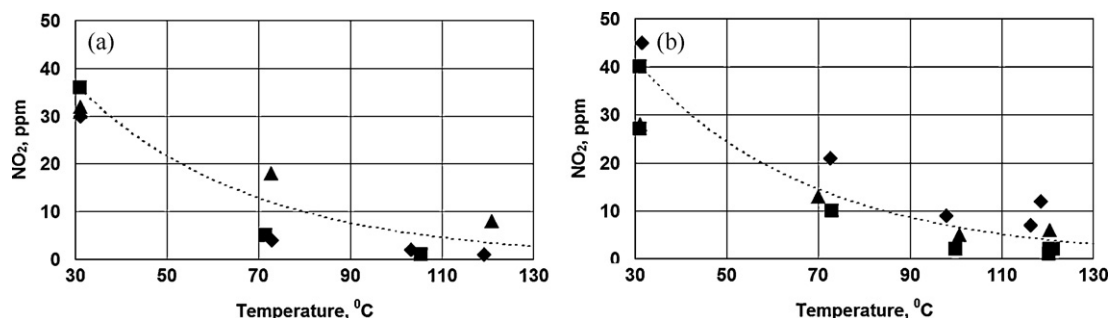


Fig. 16. Creation of NO₂ during photo-reaction at water presence in function of temperature; (a) lower water concentration below 0.7 vol.%, at high (■, 163 ± 8), medium (◆, 56 ± 5), and low (▲, 11 ± 5) C₃H₈/NO ratio; (b) higher water concentration above 1.2 vol.%, at high (■, 145 ± 12), medium (◆, 84 ± 4), and low (▲, 20 ± 5) C₃H₈/NO ratio. Data from Ref. [63].

positive influence for temperature on photo-SCR in the presence of water was recently confirmed by our research group. The photo-SCR was carried out under UV light irradiation over a PdO/TiO₂ catalyst. Significant inhibition of NO₂ generation was observed during the experiment at higher temperatures. These results are presented in Fig. 16. The left (a) and right (b) portions of the figure represent the results obtained at lower and higher concentrations of water, respectively. Increasing the temperature from 30 to 100 °C decreased NO₂ from approximately 40 to 5 ppm. Increases in temperature caused inhibition of NO₂ generation in every experiment, but the maximum deNO_x efficiency was observed in the range 70–100 °C. Further increasing the temperature decreased deNO_x efficiency. Thus, the temperature window for achieving best deNO_x efficiency was determined to be 70–100 °C. This phenomenon was explained by heterogeneous catalysis. More detailed information is available elsewhere [63].

6. Summary and remarks

The photo-deNO_x processes presented in this review are divided into three groups: photo-decomposition, photo-SCR and photo-oxidation. The photo-oxidation and photo-decomposition of NO_x were observed to behave better than photo-SCR. However, the later is still not a mature field of research capable of industrial applications. In addition, photo-SCR is more desirable than photo-oxidation because the final product of SCR is harmless N₂. Photo-decomposition is an ideal process, but it has not yet been investigated in the presence of other compounds, especially O₂ and H₂O. For this reason, we paid more attention to the influence of water and oxygen. Photo-SCR and photo-decomposition can likely be employed simultaneously, but the first one is undoubtedly more feasible for the treatment of exhaust gases. Nevertheless, some photo-NO_x removal processes have already been applied in real cases.

This review of photo-deNO_x processes also compares traditional and photo-assisted NO_x abatement methods. Although the first type of method is better known and applied more commonly in commercial systems, the photo-deNO_x method is a very attractive alternative. Photo-assisted processes are a very intensively developing area of science. The development of new deNO_x processes is an urgent task. This area of research is not only interesting to scientists, but is also critical for the development of “green environmental processes”.

The combination of thermal (traditional) and photocatalytic deNO_x can be synergistic and should be explored for the abatement of poisonous substance emissions. We believe that photocatalysis can enhance these efforts. One of the main challenges for scientists is to obtain a stable photocatalyst that is active under visible light. As a result, intensive investigations in this aspect are still ongoing. The development of new photocatalysts that are

active under visible light will make the entire process more effective and affordable because sunlight is an abundant and powerful source of energy.

7. Sources of further information

Photocatalytic removal of NO_x can often be found in commercial air cleaning processes. Commercial markets offer many products for the photo-oxidation of NO_x and others pollutants [180]. Additionally, commercial laboratories specialize in the testing of photocatalysts used for deNO_x. The Photocatalyst Section at the Environmental Technical Laboratory Ltd, Japan details the tests used to assess photocatalytic materials in nitrogen oxide removal [181]. Some companies recommend TiO₂ as a good photocatalyst for NO_x and other pollutants removal (e.g., Belgian Road Research Centre [182], TitanPE Technologies Inc. [183], Bio Shield, Inc. [184], and Górażdże CEMENT SA, Poland [185]). Photocatalytic deNO_x processes are also prominently featured on quasi-science websites (e.g., [186]).

Acknowledgements

This work was financially supported by the National Science Council of Taiwan under project NSC98-2911-I-002-002. We would like to thank Raymond Liao for help with writing. Janusz Lasek would like to thank Prof. Jeffrey Chi-Sheng Wu for the invitation and supervision of a one-year post-doctoral project at the National Taiwan University.

References

- [1] J.-T. Lin, M.B. McElroy, K.F. Boersma, *Atmos. Chem. Phys.* 10 (2010) 63–78.
- [2] F. Normann, K. Andersson, B. Leckner, F. Johnsson, *Prog. Energy Combust. Sci.* 35 (2009) 385–397.
- [3] S. Roy, M.S. Hegde, G. Madras, *Appl. Energy* 86 (2009) 2283–2297.
- [4] M. Danesh Miah, M. Farhad Hossain Masum, M. Koike, *Energy Policy* 38 (2010) 4643–4651.
- [5] K. Skalska, J.S. Miller, S. Ledakowicz, *Sci. Total Environ.* 408 (2010) 3976–3989.
- [6] Y. Sadanaga, J. Matsumoto, Y. Kajii, *J. Photochem. Photobiol. C* 4 (2003) 85–104.
- [7] B. Chen, C. Hong, H. Kan, *Toxicology* 198 (2004) 291–300.
- [8] P.E. Morrow, *J. Toxicol. Environ. Health* 13 (1984) 205–227.
- [9] J.A. Last, W.M. Sun, H. Witschi, *Environ. Health Perspect.* 102 (1994) 179–184.
- [10] S.A. Cormier, S. Lomnicki, W. Backes, B. Dellinger, *Environ. Health Perspect.* 114 (2006).
- [11] V. Mohsenin, *Toxicology* 89 (1994) 301–312.
- [12] R. de Richter, S. Caillol, *J. Photochem. Photobiol. C* 12 (2011) 1–19.
- [13] P. Glarborg, A.D. Jensen, J.E. Johnsson, *Prog. Energy Combust. Sci.* 29 (2003) 89–113.
- [14] B. Gradoń, *Zeszyty naukowe Politechniki Śląskiej, Hutnictwo*, 67, 2003.
- [15] Y.B. Zeldovich, *Acta Physicochem. USSR*. 21 (1946) 577–628.
- [16] J. Wolfrum, *Chemie Ingenieur Technik* 44 (1972) 656–659.
- [17] P.C. Malte, D.T. Pratt, *Combust. Sci. Technol.* 9 (1974) 221–231.
- [18] J. Tomeczek, B. Gradoń, *Combust. Flame* 133 (2003) 311–322.
- [19] J. Tomeczek, B. Gradoń, *Combust. Sci. Technol.* 125 (1997) 159–180.
- [20] C.P. Fenimore, *Proceedings of the Combustion Institute*, 1971, pp. 373–380.

- [21] J.W. Bozzelli, A.M. Dean, *Int. J. Chem. Kinet.* 27 (1995) 1097–1109.
- [22] J.A. Sutton, J.W. Fleming, *Combust. Flame* 154 (2008) 630–636.
- [23] K. Okazaki, T. Ando, *Energy* 22 (1995) 207–215.
- [24] L. Shi, Y. Cui, K. Deng, H. Peng, Y. Chen, *Energy* 31 (2006) 2665–2676.
- [25] J. Tomczek, *Hutnik* 7 (1994) 235–238.
- [26] M.B. Toftegaard, J. Brix, P.A. Jensen, P. Glarborg, A.D. Jensen, *Prog. Energy Combust. Sci.* 36 (2010) 581–625.
- [27] M. Flamme, *Energy Convers. Manage.* 42 (2001) 1919–1935.
- [28] Y.D. Wang, D. McIlveen-Wright, Y. Huang, N. Hewitt, P. Eames, S. Rezvani, J. McMullan, A.P. Roskilly, *Fuel* 86 (2007) 2101–2108.
- [29] J. Tomczek, J. Góral, B. Gradoń, *J. Energy Inst.* 68 (1995) 178–183.
- [30] J.M. López, F. Jiménez, F. Aparicio, N. Flores, *Transport. Res. D: Trans. Environ.* 14 (2009) 1–5.
- [31] E. Rajasekar, A. Murugesan, R. Subramanian, N. Nedunchezian, *Renew. Sust. Energ. Rev.* 14 (2010) 2113–2121.
- [32] J. Xu, X. Zhang, J. Liu, L. Fan, *Int. J. Hydrogen Energy* 35 (2010) 2909–2914.
- [33] W. Nimmo, A.A. Patsias, E. Hampartsoumian, B.M. Gibbs, M. Fairweather, P.T. Williams, *Fuel* 83 (2004) 1143–1150.
- [34] V.V. Lissianski, V.M. Zamansky, P.M. Maly, *Combust. Flame* 125 (2001) 1118–1127.
- [35] V.I. Pärvulescu, P. Grange, B. Delmon, *Catal. Today* 46 (1998) 233–316.
- [36] S. Bröer, T. Hammer, *Appl. Catal. B* 28 (2000) 101–111.
- [37] P. Forzatti, *Appl. Catal. A* 222 (2001) 221–236.
- [38] R.M. Heck, R.J. Farrauto, *Appl. Catal. A* 221 (2001) 443–457.
- [39] D. Chatterjee, P. Kočí, V. Schmeißer, M. Marek, M. Weibel, B. Krutzsch, *Catal. Today* 151 (2010) 395–409.
- [40] S.W. Bae, S.A. Roh, S.D. Kim, *Chemosphere* 65 (2006) 170–175.
- [41] Y. Li, Y. Liu, L. Zhang, Q. Su, G. Jin, *Chin. J. Chem. Eng.* 18 (2010) 244–248.
- [42] B.-R. Deshwal, H.-K. Lee, *J. Environ. Sci.* 21 (2009) 155–161.
- [43] Y.S. Mok, *J. Chem. Eng. Jpn.* 37 (2004) 1337–1344.
- [44] Y.S. Mok, H.-J. Lee, *Fuel Process. Technol.* 87 (2006) 591–597.
- [45] J. Mo, Y. Zhang, Q. Xu, J.J. Lamson, R. Zhao, *Atmos. Environ.* 43 (2009) 2229–2246.
- [46] J. Zhao, X. Yang, *Build. Environ.* 38 (2003) 645–654.
- [47] P. Pichat, J.-M. Herrmann, H. Courbon, J. Disdier, M.-N. Mozzanega, *Can. J. Chem. Eng.* 60 (1982) 27–32.
- [48] H. Courbon, P. Pichat, *J. Chem. Soc. Faraday Trans. 1: Phys. Chem. Condensed Phases* 80 (1984) 3175–3185.
- [49] Y. Yokomichi, T. Nakayama, O. Okada, Y. Yokoi, I. Takahashi, H. Uchida, H. Ishikawa, R. Yamaguchi, H. Matsui, T. Yamabe, *Catal. Today* 29 (1996) 155–160.
- [50] W.-S. Ju, M. Matsuoka, M. Anpo, *Catal. Lett.* 71 (2001) 91–93.
- [51] W.-S. Ju, M. Matsuoka, M. Anpo, *Int. J. Photoenergy* 05 (2003) 17–19.
- [52] K.H. Kim, et al., *J. Phys.: Condens. Matter* 22 (2010) 084012.
- [53] M. Matsuoka, W.-S. Ju, M. Anpo, *Chem. Lett.* 29 (2000) 626–627.
- [54] S. Poulston, M.V. Twigg, A.P. Walker, *Appl. Catal. B* 89 (2009) 335–341.
- [55] S. Roy, T. Aarthi, M.S. Hegde, G. Madras, *Ind. Eng. Chem. Res.* 46 (2007) 5798–5802.
- [56] S. Roy, M.S. Hegde, N. Ravishanker, G. Madras, *J. Phys. Chem. C* 111 (2007) 8153–8160.
- [57] N. Bowering, D. Croston, P.G. Harrison, G.S. Walker, *Int. J. Photoenergy* 2007 (2007) 1–8.
- [58] N. Bowering, G.S. Walker, P.G. Harrison, *Appl. Catal. B* 62 (2006) 208–216.
- [59] M. Matsuoka, S. Higashimoto, H. Yamashita, M. Anpo, *Res. Chem. Intermediates* 26 (2000) 87–92.
- [60] I.H. Su, J.C.S. Wu, *Catal. Commun.* 10 (2009) 1534–1537.
- [61] R.K. Thampi, P. Ruterana, M. Grätzel, *J. Catal.* 126 (1990) 572–590.
- [62] Y.-H. Yu, Y.-T. Pan, Y.-T. Wu, J. Lasek, J.C.S. Wu, *Catal. Today* 174 (2011) 141–147.
- [63] J. Lasek, Y.-H. Yu, J.C.S. Wu, *Environ. Technol.* (2012) 1–9.
- [64] S. Yamazoe, Y. Masutani, K. Teramura, Y. Hitomi, T. Shishido, T. Tanaka, *Appl. Catal. B: Environ.* 83 (2008) 123–130.
- [65] S. Yamazoe, Y. Masutani, T. Shishido, T. Tanaka, *Res. Chem. Intermediate* 34 (2008) 487–494.
- [66] K. Teramura, T. Tanaka, S. Yamazoe, K. Arakaki, T. Funabiki, *Appl. Catal. B* 53 (2004) 29–36.
- [67] R. Jin, Z. Wu, Y. Liu, B. Jiang, H. Wang, *J. Hazard. Mater.* 161 (2009) 42–48.
- [68] N.W. Cant, J.R. Cole, *J. Catal.* 134 (1992) 317–330.
- [69] M. Anpo, T.-H. Kim, M. Matsuoka, *Catal. Today* 142 (2009) 114–124.
- [70] K. Takeuchi, T. Yazawa, T. Ibusuki, *Atmos. Environ.* (1967) 17 (1983) 2253–2258.
- [71] K. Takeuchi, T. Ibusuki, *Atmos. Environ.* (1967) 20 (1986) 1155–1160.
- [72] Y. Hu, M. Matsuoka, M. Anpo, *Mater. Sci. Forum* 510–511 (2006) 82–85.
- [73] K. Teramura, T. Tanaka, T. Funabiki, *Langmuir* 19 (2003) 1209–1214.
- [74] Y. Ohko, Y. Nakamura, N. Negishi, S. Matsuzawa, K. Takeuchi, *J. Photochem. Photobiol. A* 205 (2009) 28–33.
- [75] S. Yin, Y. Aita, M. Komatsu, J. Wang, Q. Tang, T. Sato, *J. Mater. Chem.* 15 (2005) 674–682.
- [76] Y. Ishibai, J. Sato, S. Akita, T. Nishikawa, S. Miyagishi, *J. Photochem. Photobiol. A* 188 (2007) 106–111.
- [77] M.M. Ballari, M. Hunger, G. Hüsken, H.J.H. Brouwers, *Appl. Catal. B* 95 (2010) 245–254.
- [78] M. Hunger, G. Hüsken, H.J.H. Brouwers, *Cem. Concr. Res.* 40 (2010) 313–320.
- [79] B.N. Shelimov, N.N. Tolkachev, O.P. Tkachenko, G.N. Baeva, K.V. Klemen-tiev, A.Y. Stakheev, V.B. Kazansky, *J. Photochem. Photobiol. A* 195 (2008) 81–88.
- [80] J. Zhang, T. Ayusawa, M. Minagawa, K. Kinugawa, H. Yamashita, M. Matsuoka, M. Anpo, *J. Catal.* 198 (2001) 1–8.
- [81] Z. Sheng, Z. Wu, Y. Liu, H. Wang, *Catal. Commun.* 9 (2008) 1941–1944.
- [82] Z. Wu, Z. Sheng, Y. Liu, H. Wang, N. Tang, J. Wang, *J. Hazard. Mater.* 164 (2009) 542–548.
- [83] Z. Wu, Z. Sheng, H. Wang, Y. Liu, *Chemosphere* 77 (2009) 264–268.
- [84] S. Matsuda, H. Hatano, A. Tsutsumi, *J. Chem. Eng.* 82 (2001) 183–188.
- [85] S. Yin, B. Liu, P. Zhang, T. Morikawa, K.-I. Yamanaka, T. Sato, *J. Phys. Chem. C* 112 (2008) 12425–12431.
- [86] S. Yin, H. Yamaki, M. Komatsu, Q. Zhang, J. Wang, Q. Tang, F. Saito, T. Sato, *Solid State Sci.* 7 (2005) 1479–1485.
- [87] C.-H. Huang, I.K. Wang, Y.-M. Lin, Y.-H. Tseng, C.-M. Lu, *J. Mol. Catal. A: Chem.* 316 (2010) 163–170.
- [88] Y.-H. Tseng, et al., *Nanotechnology* 17 (2006) 2490.
- [89] K. Hashimoto, K. Sumida, S. Kitano, K. Yamamoto, N. Kondo, Y. Kera, H. Kominami, *Catal. Today* 144 (2009) 37–41.
- [90] J.S. Dalton, P.A. Janes, N.G. Jones, J.A. Nicholson, K.R. Hallam, G.C. Allen, *Environ. Pollut.* 120 (2002) 415–422.
- [91] Y. Komazaki, H. Shimizu, S. Tanaka, *Atmos. Environ.* 33 (1999) 4363–4371.
- [92] T. Ibusuki, K. Takeuchi, *J. Mol. Catal.* 88 (1994) 93–102.
- [93] I. Nakamura, N. Negishi, S. Kutsuna, T. Ihara, S. Sugihara, K. Takeuchi, *J. Mol. Catal. A: Chem.* 161 (2000) 205–212.
- [94] C.H. Ao, S.C. Lee, C.L. Mak, L.Y. Chan, *Appl. Catal. B* 42 (2003) 119–129.
- [95] C.H. Ao, S.C. Lee, *Appl. Catal. B* 44 (2003) 191–205.
- [96] F.L. Toma, G. Bertrand, D. Klein, C. Coddet, *Environ. Chem. Lett.* 2 (2004) 117–121.
- [97] F.-L. Toma, S. Guessasma, D. Klein, G. Montavon, G. Bertrand, C. Coddet, *J. Photochem. Photobiol. A* 165 (2004) 91–96.
- [98] S. Devahasdin, C. Fan, K. Li, D.H. Chen, *J. Photochem. Photobiol. A* 156 (2003) 161–170.
- [99] H. Wang, Z. Wu, W. Zhao, B. Guan, *Chemosphere* 66 (2007) 185–190.
- [100] F.-L. Toma, G. Bertrand, S.O. Chwa, D. Klein, H. Liao, C. Meunier, C. Coddet, *Mater. Sci. Eng. A* 417 (2006) 56–62.
- [101] F.-L. Toma, D. Sokolov, G. Bertrand, D. Klein, C. Coddet, C. Meunier, *J. Therm. Spray Technol.* 15 (2006) 576–581.
- [102] F.-L. Toma, G. Bertrand, S.O. Chwa, C. Meunier, D. Klein, C. Coddet, *Surf. Coat. Technol.* 200 (2006) 5855–5862.
- [103] F.-L. Toma, G. Bertrand, D. Klein, C. Meunier, S. Begin, *J. Nanomater.* 2008 (2008) 1–8.
- [104] K. Hashimoto, K. Wasada, M. Osaki, E. Shono, K. Adachi, N. Toukai, H. Kominami, Y. Kera, *Appl. Catal. B* 30 (2001) 429–436.
- [105] Q.L. Yu, H.J.H. Brouwers, *Appl. Catal. B* 92 (2009) 454–461.
- [106] F. Spadavecchia, G. Cappelletti, S. Arizzzone, C.L. Bianchi, S. Cappelli, C. Oliva, P. Scardi, M. Leoni, P. Fermo, *Appl. Catal. B* 96 (2010) 314–322.
- [107] M. Signoretto, E. Ghedini, V. Trevisan, C.L. Bianchi, M. Ongaro, G. Cruciani, *Appl. Catal. B* 95 (2010) 130–136.
- [108] C. Cacho, O. Geiss, J. Barrero-Moreno, V.D. Binas, G. Kiriakidis, L. Botalico, D. Kotzias, *J. Photochem. Photobiol. A* 222 (2011) 304–306.
- [109] T. Martinez, A. Bertron, E. Ringot, G. Escadellias, *Build. Environ.* 46 (2011) 1808–1816.
- [110] X. Ding, X. Song, P. Li, Z. Ai, L. Zhang, *J. Hazard. Mater.* 190 (2011) 604–612.
- [111] Y.-H. Tseng, C.-H. Kuo, *Catal. Today* 174 (2011) 114–120.
- [112] J.C.S. Wu, Y.-T. Cheng, *J. Catal.* 237 (2006) 393–404.
- [113] Q.L. Yu, M.M. Ballari, H.J.H. Brouwers, *Appl. Catal. B: Environ.* 99 (2010) 58–65.
- [114] A. Folli, S.B. Campbell, J.A. Anderson, D.E. Macphee, *J. Photochem. Photobiol. A* 220 (2011) 85–93.
- [115] S. Chin, E. Park, M. Kim, J. Jeong, G.-N. Bae, *J. Jurng. Powder Technol.* 206 (2011) 306–311.
- [116] Z. Wu, Z. Sheng, Y. Liu, H. Wang, J. Mo, *J. Hazard. Mater.* 185 (2011) 1053–1058.
- [117] K. Hashimoto, K. Wasada, N. Toukai, H. Kominami, Y. Kera, *J. Photochem. Photobiol. A* 136 (2000) 103–109.
- [118] H. Yamashita, Y. Ichihashi, S.G. Zhang, Y. Matsumura, Y. Souma, T. Tatsumi, M. Anpo, *Appl. Surf. Sci.* 121–122 (1997) 305–309.
- [119] M. Anpo, M. Takeuchi, K. Ikeue, S. Dohshi, *Curr. Opin. Solid State Mater. Sci.* 6 (2002) 381–388.
- [120] M. Anpo, M. Takeuchi, *J. Catal.* 216 (2003) 505–516.
- [121] M. Takeuchi, H. Yamashita, M. Matsuoka, M. Anpo, T. Hirao, N. Itoh, N. Iwamoto, *Catal. Lett.* 67 (2000) 135–137.
- [122] M. Anpo, *Pure Appl. Chem.* 72 (2000) 1787–1792.
- [123] M. Anpo, M. Matsuoka, H. Yamashita, W.-S. Ju, S.-E. Park, Y.-G. Shul, *J. Ind. Eng. Chem.* 6 (2000) 133–143.
- [124] N. Negishi, M. Matsuoka, H. Yamashita, M. Anpo, *J. Phys. Chem.* 97 (1993) 5211–5212.
- [125] T.H. Lim, S.M. Jeong, S.D. Kim, J. Gyenis, *J. Photochem. Photobiol. A* 134 (2000) 209–217.
- [126] M. Anpo, M. Matsuoka, H. Yamashita, *Catal. Today* 35 (1997) 177–181.
- [127] M. Anpo, S.G. Zhang, H. Mishima, M. Matsuoka, H. Yamashita, *Catal. Today* 39 (1997) 159–168.
- [128] J. Zhang, Y. Hu, M. Matsuoka, H. Yamashita, M. Minagawa, H. Hidaka, M. Anpo, *J. Phys. Chem. B* 105 (2001) 8395–8398.
- [129] J. Zhang, M. Minagawa, T. Ayusawa, S. Natarajan, H. Yamashita, M. Matsuoka, M. Anpo, *J. Phys. Chem. B* 104 (2000) 11501–11505.
- [130] Y. Hu, S. Higashimoto, G. Martra, J. Zhang, M. Matsuoka, S. Coluccia, M. Anpo, *Catal. Lett.* 90 (2003) 161–163.
- [131] M. Anpo, Y. Ichihashi, M. Takeuchi, H. Yamashita, *Res. Chem. Intermed.* 24 (1998) 143–149.

- [132] M. Anpo, M. Takeuchi, *Int. J. Photoenergy* 3 (2001) 89–94.
- [133] M. Anpo, *Pure Appl. Chem.* 72 (2000) 1265–1270.
- [134] M. Anpo, S.G. Zhang, S. Higashimoto, M. Matsuoka, H. Yamashita, Y. Ichihashi, Y. Matsumura, Y. Souma, *J. Phys. Chem. B* 103 (1999) 9295–9301.
- [135] M. Anpo, *Sol. Energy Mater. Sol. Cells* 38 (1995) 221–238.
- [136] S. Zhang, N. Fujii, Y. Nosaka, *J. Mol. Catal. A: Chem.* 129 (1998) 219–224.
- [137] B. Klotz, Summary of Presentations at the US/German – Environmental Chamber Workshop, Riverside, CA, October 4–6, 1999, pp. 1–13.
- [138] J. Zádor, T. Turányi, K. Wirtz, M. Pilling, *J. Atmos. Chem.* 55 (2006) 147–166.
- [139] B. Zielinska, J. Sagebiel, W. Stockwell, J. McDonald, J. Seagrave, P. Wiesen, K. Wirtz, Investigation of Atmospheric Transformations of Diesel Emissions in the European Photoreactor (EUPHORE), in: I. Barnes, K. Rudzinski (Eds.), *Environmental Simulation Chambers: Application to Atmospheric Chemical Processes*, Springer, Netherlands, 2006, pp. 279–284.
- [140] B. Zielinska, *Exp. Toxicol. Pathol.* 57 (2005) 31–42.
- [141] T. Maggos, J.G. Bartzis, P. Leva, D. Kotzias, *Appl. Phys. A* 89 (2007) 81–84.
- [142] T. Maggos, J.G. Bartzis, M. Liakou, C. Gobin, *J. Hazard. Mater.* 146 (2007) 668–673.
- [143] T. Maggos, A. Plassais, J. Bartzis, C. Vasilakos, N. Moussiopoulos, L. Bonafous, *Environ. Monit. Assess.* 136 (2008) 35–44.
- [144] D.H. Chen, K. Li, R. Yuan, Annual Project Report Submitted to Houston Advanced Research Center and Office of Air Quality Planning and Standards. U.S. Environmental Protection Agency, Research Triangle Park, NC 27711, 2007, pp. 1–17.
- [145] G.L. Guerrini, F. Corazza, First Arab International Conference and Exhibition on The Uses of White Cement, Cairo, Egypt, 28–30 April 2008.
- [146] S. Guo, Z. Wu, W. Zhao, *Chin. Sci. Bull.* 54 (2009) 1137–1142.
- [147] H. Taoda, *Synthesiology* 1 (2008) 287–295 (translation from Japanese).
- [148] H. Hamada, K.-i. Komure, R. Takahashi, T. Yamaji, RILEM International Symposium on Environment-Conscious Materials and Systems for Sustainable Development, September 6–7, 2004, Koriyama, Japan, 2004, pp. 361–366.
- [149] A. Fujishima, X. Zhang, *Comptes Rendus Chimie* 9 (2006) 750–760.
- [150] O. Carp, C.L. Huisman, A. Reller, *Prog. Solid State Chem.* 32 (2004) 33–177.
- [151] L. Venturini, M. Bacchi, II International Conference Environmentally Friendly Roads Enviroad, Warsaw, Poland October 15–16, 2009.
- [152] S. Laufs, G. Burgeth, W. Duttlinger, R. Kurtenbach, M. Maban, C. Thomas, P. Wiesen, J. Kleffmann, *Atmos. Environ.* 44 (2010) 2341–2349.
- [153] M. Chen, J.-W. Chu, *J. Cleaner Product.* 19 (2011) 1266–1272.
- [154] Y. Paz, *Appl. Catal. B* 99 (2010) 448–460.
- [155] M. Hayakawa, M. Chikuni, T. Watanabe, United States Patent 6,191,062 (2001).
- [156] K. Tsujimichi, H. Hasuo, H. Kobayashi, United States Patent 0036897 (2001).
- [157] M. Ohmori, H. Nakamura, N. Murase, N. Uotani, T. Ohkubo, United States Patent 6,337,301 (2002).
- [158] I.C. Gambarelli, G. Pozzi, United States Patent 7,608,297 (2009).
- [159] S. Sugihara, United States Patent 6,908,881 (2005).
- [160] Y. Aido, Japan Patent 924 846 6 (1997).
- [161] Z.J. Ji, X.W. Yan, J. Wang, China Patent 1597091 (2005).
- [162] S.H. Han, Korean Patent 0007840 (2009).
- [163] K. Huder, German Patent 41 10227 (1992).
- [164] H. Taoda, Y. Yamada, K. Aizawa, United States Patent 6,508,992 (2003).
- [165] H. Taoda, Y. Yamada, K. Aizawa, United States Patent 6,838,059 (2005).
- [166] T. Kagitani, K. Doi, T. Azuma, Japan Patent 55,015,637 (1980).
- [167] Z.W. Wu, China Patent 1,883,775 (2006).
- [168] K. Kawai, M. Tatsumi, United States Patent 7,468,529 (2008).
- [169] K. Hokkirigawa, N. Yoshimura, J. Hirose, United States Patent 0031642 A1 (2004).
- [170] K. Hokkirigawa, N. Yoshimura, J. Hirose, European Patent 1369532 A2 (2003).
- [171] D. Schwaag, Great Britain Patent 2,441,171 (2008).
- [172] T. Saito, T. Ogawa, A. Kushibe, S. Ando, Y. Ito, Japan Patent 10331116 (1998).
- [173] N. Shigaya, Japan Patent 254,322 (2001).
- [174] M. Miyauchi, A. Nakajima, K. Hashimoto, T. Watanabe, *Adv. Mater.* 12 (2000) 1923–1927.
- [175] M. Miyauchi, A. Nakajima, T. Watanabe, K. Hashimoto, *Chem. Mater.* 14 (2002) 2812–2816.
- [176] A. Hoffmann, J. Grossmann, R. Zellner, *J. Photochem. Photobiol. A* 176 (2005) 260–269.
- [177] H. Muto, Y. Takizawa, *Chemosphere* 21 (1990) 1423–1428.
- [178] T. Ibusuki, K. Takeuchi, *Atmos. Environ.* (1967) 20 (1986) 1711–1715.
- [179] H. Takagi, N. Washida, H. Akimoto, K. Nagasawa, Y. Usui, M. Okuda, *J. Phys. Chem.* 84 (1980) 478–483.
- [180] <http://www.alibaba.com/products/tio2/613.html?noddp=Y>, website 31.05.2010.
- [181] http://www.etlabo.co.jp/en/image/photocatalytic_materials.pdf, Website 31.05.2010.
- [182] A. Beeldens, http://www.brcc.be/pdf/tra/tra_beeldens.txt.pdf, Website 31.05.2010.
- [183] <http://www.tipe.com.cn/index.htm>.
- [184] http://www.teamenviroclean.com/chemistry_of_tio2_nanotechnology, website 31.05.2010.
- [185] <http://www.gorazdze.pl>, website 31.05.2010.
- [186] <http://odpady.org.pl/plugins/content/content.php?content.2134.1>, website 31.05.2010.
- [187] I.T.A. Harrick Scientific Products, 2nd Floor, Pleasantville, NY 10570, U.S. (Ed.), 2003, pp. 9–18.